Deterministic strong-field quantum control

Stefano M. Cavaletto,* Zoltán Harman, Thomas Pfeifer, and Christoph H. Keitel
Max-Planck-Institut für Kernphysik, Saupfercheckweg 1, 69117 Heidelberg, Germany
(Received 15 July 2016; revised manuscript received 1 February 2017; published 17 April 2017)

Strong-field quantum-state control is investigated, taking advantage of the full—amplitude and phase—characterization of the interaction between matter and intense ultrashort pulses via transient-absorption spectroscopy. As an example, we apply the method to a nondegenerate V-type three-level system modeling atomic Rb, and use a sequence of intense delayed pulses, whose parameters are tailored to steer the system into a desired quantum state. We show how to experimentally enable this optimization by retrieving all quantum features of the light-matter interaction from observable spectra. This provides a full characterization of the action of strong fields on the atomic system, including the dependence upon possibly unknown pulse properties and atomic structures. Precision and robustness of the scheme are tested, in the presence of surrounding atomic levels influencing the system's dynamics.

DOI: 10.1103/PhysRevA.95.043413

I. INTRODUCTION

The advent of laser light and femtosecond pulse-shaping technology have revolutionized our access to the quantum properties of matter [1–3], with coherent-control methods exploiting interference in order to steer a system into a given state with light [4–8]. Measurement-driven techniques such as adaptive feedback control are extensively used, especially when little understanding of the light-matter interaction is available owing to inaccurately known atomic or molecular structures, nonideal experimental conditions, or because of the use of strong, insufficiently characterized laser fields. Femtosecond pulses are thus utilized to simultaneously control and interrogate the atomic system, with their shape being iteratively optimized based on the received experimental response [5]. However, the associated atomic dynamics remain concealed in the optimal pulse, often preventing insight into the underlying physical mechanism. Only recently techniques were investigated to access the complex reaction pathways followed by an optimally controlled system [9,10] and in the strong-field regime, where perturbative approaches fail and the atomic level structure is dressed by the time-dependent field, a limited number of effective pulse-shaping strategies have been identified [11–14].

Major advances in x-ray free-electron lasers (FELs) are now enabling quantum control also at short wavelengths [15]. Coherent transform-limited x-ray pulses are produced via seeding methods at FELs [16,17], opening the field of x-ray quantum optics [18]. Despite recent advances [19,20], however, experimental challenges still need to be faced. Complex spectral-shaping methods are not yet available at short wavelengths, in particular for hard x rays, and control schemes, e.g., to manipulate several excited states lying within the x-ray pulse bandwidth, should preferably rely on optimal pulse sequences. Methods to measure pulse temporal profiles are significantly hindered at x-ray frequencies by the absence of suitable nonlinear crystals. Therefore, measurement-driven strategies directly accessing the atomic response to intense, insufficiently characterized pulses should be preferred to methods based on theoretical assumptions of the pulse shape. At the same time, the reduced flexibility at recently established x-ray FELs renders adaptive feedback still very challenging for current experiments.

In order to determine an effective route to x-ray quantum control despite present limitations, we put forward a scheme to experimentally characterize—in amplitude and phase—the atomic interaction with intense ultrashort pulses, and use this information to deterministically guide the system into a desired state with an optimal pulse sequence [Fig. 1(a)]. Thereby, one keeps the advantages of a measurement-driven strategy. In stark contrast to adaptive feedback, however, where optimal pulse shapes are iteratively determined via a trial-and-error procedure, our scheme allows access and visualization of the building blocks constituting the optimal strong-field control strategy, providing an advantageous means to unravel the dynamical pathways followed by the system. Furthermore, for experimental conditions in which feedback may not be advisable due to, e.g., restricted beam time, our scheme represents a cost-effective strategy to prepare a given system in different states: adaptive feedback requires a new sequence of iterations for every desired state, whereas deterministic strong-field control could be performed numerically relying on a set of elementary steps characterized experimentally. Motivated by recent results [21], the scheme is applied here to control optical transitions in Rb atoms, but it could be also implemented at x-ray energies with, e.g., highly charged ions, among the best candidates for future x-ray quantum-optics applications [18].

The paper is structured as follows. In Sec. II, we take advantage of a Schrödinger-equation-based formalism to introduce the interaction operators, which will be used to characterize the atomic response to intense ultrashort pulses. We introduce transient-absorption spectroscopy in Sec. III, and show in Sec. IV how this can be employed to reconstruct strong-field interaction operators. These extracted operators are used in Sec. V for deterministic strong-field quantum control, and the performances of the scheme, also in the presence of incomplete modeling, are discussed in Sec. VI. All the results are generalized in terms of a density-matrix formalism in Sec. VII, in order to fully account for the details of dissipation. Section VIII concludes the paper. Atomic units are used unless stated otherwise.

*smcavaletto@gmail.com

 ©2017 American Physical Society

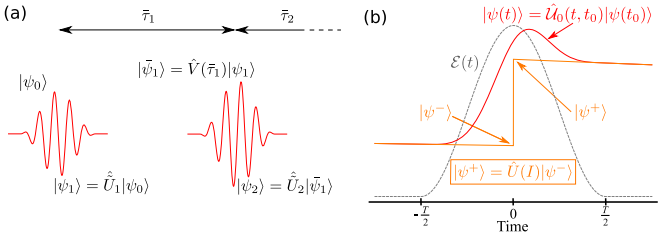

FIG. 1. (a) Quantum-control scheme based on an optimal sequence of experimentally characterized pulses. (b) Interaction of a quantum system (red, continuous line) with an ultrashort pulse (gray, dashed line), effectively modeled as an instantaneous effect (orange, continuous line).

II. INTERACTION OPERATORS

The key quantity we will use to characterize the atomic response to intense ultrashort pulses is the interaction operator $\hat{U}(I)$, whose action is represented in Fig. 1(b). Thereby, we can effectively describe the atomic evolution induced by the pulse as a δ-like interaction [22,23], where $\hat{U}(I)$ connects the *effective* initial and final states of the atomic system, $|\psi^-\rangle$ and $|\psi^+\rangle$, respectively, preceding and following the interaction with an ultrashort pulse of intensity I:

$$|\psi^+\rangle = \hat{U}(I)|\psi^-\rangle. \tag{1}$$

Our deterministic strong-field control method consists in (a) extracting $\hat{U}(I)$ from experimental spectra and (b) designing the optimal pulse sequence of Fig. 1(a) based on this reconstructed information, in order to guide the atomic system into a desired state $|\psi_\mathrm{d}\rangle$. In adaptive feedback, a series of experiments has to be performed for every choice of $|\psi_\mathrm{d}\rangle$, iteratively searching for the optimal combinations of, e.g., pulse delays, carrier-envelope phases (CEPs), and intensities. Little knowledge is thereby achieved about the possible pathways the system could follow and the rules determining the optimal pulse sequence. In contrast, in deterministic strong-field control, experiments are first run to fully characterize the interaction operators $\hat{U}(I)$, providing a complete experimental mapping of the available control options and facilitating manipulation and interpretation of the chosen control strategy. Although interaction operators could be calculated from theory, our deterministic scheme allows one to effectively tackle those cases where reliable predictions are not possible via methods based exclusively on theory, due to missing knowledge of the atomic structures, pulse shapes, or the strong-field interaction.

In order to define the interaction operator $\hat{U}(I)$ and extract it from measurable absorption spectra, we therefore consider a quantum system in the state $|\psi(t)\rangle = \hat{\mathcal{U}}(t,t_0)|\psi(t_0)\rangle$, where the evolution operator $\hat{\mathcal{U}}(t,t_0)$, describing the dynamics from t_0 to t, is solution of the Schrödinger equation

$$\frac{d\hat{\mathcal{U}}(t,t_0)}{dt} = -i[\hat{H}_0 + \hat{H}_\mathrm{int}]\hat{\mathcal{U}}(t,t_0), \quad \hat{\mathcal{U}}(t_0,t_0) = \hat{I}. \tag{2}$$

We employ a Schrödinger-like approach, where we include the decay of the excited levels via the complex-valued atomic-structure Hamiltonian $\hat{H}_0 = \sum_i (\omega_i - i\gamma_i/2)|i\rangle\langle i|$, with energies ω_i and linewidths γ_i of each atomic state $|i\rangle$. In Sec. VII, the results of the paper are generalized via a density-matrix formalism, in order to fully include the details of dissipation. In Eq. (2), $\hat{I} = \sum_i |i\rangle\langle i|$ is the identity operator and $\hat{H}_\mathrm{int} = -[\hat{\boldsymbol{D}}^- \cdot \boldsymbol{\mathcal{E}}^+(t) + \mathrm{H.c.}]$ is the electric-dipole ($E1$) light-matter interaction Hamiltonian, in the rotating-wave approximation [24]. Here, $\hat{\boldsymbol{D}}^- = \sum_{i>j} \boldsymbol{D}_{ij}|i\rangle\langle j|$ is the negative-frequency part of the dipole-moment operator, of matrix elements $\boldsymbol{D}_{ij}$, and $\boldsymbol{\mathcal{E}}^+(t)$ is the complex electric field [25]. We assume a quantum-control scheme based on pulses of the form $\boldsymbol{\mathcal{E}}(t) = \boldsymbol{\mathcal{E}}^+(t) + \mathrm{c.c.} = \mathcal{E}_0\, f(t-t_\mathrm{c})\cos[\omega_\mathrm{L}(t-t_\mathrm{c}) + \phi]\hat{\boldsymbol{e}}_z$, centered around t_c, linearly polarized along the $\hat{\boldsymbol{e}}_z$ unit vector, with laser frequency $\omega_\mathrm{L} = 1.59$ eV and CEP ϕ. The envelope function $f(t)$ is nonvanishing in the interval $[-T/2, T/2]$, with pulse duration T, and $\mathcal{E}_0 = \sqrt{8\pi\alpha I}$ represents the peak field strength, with peak intensity I and the fine-structure constant α.

The evolution operator $\hat{\mathcal{U}}(t,t_0)$ satisfies the equality $\hat{\mathcal{U}}(t,t_0) = \hat{\mathcal{U}}(t,s)\hat{\mathcal{U}}(s,t_0)$, from which it follows that, since $\hat{\mathcal{U}}(t_0,t_0) = \hat{I}$, its inverse is given by $\hat{\mathcal{U}}^{-1}(t,t_0) = \hat{\mathcal{U}}(t_0,t)$. In the absence of external fields, the known free evolution of the system under the action of the atomic-structure Hamiltonian $\hat{H}_0$ is given by $\hat{V}(t) = e^{-i\hat{H}_0 t}$, with $\hat{V}^{-1}(t) = \hat{V}(-t)$. In order to effectively describe the action of a pulse on the atomic system as a function of its intensity, we initially consider pulses centered on $t_\mathrm{c} = 0$ and with vanishing CEP, associated with the evolution operator $\hat{\mathcal{U}}_0(t,t_0)$. The generic evolution operator $\hat{\mathcal{U}}(t,t_0) = \hat{\Phi}^\dagger(\phi)\hat{\mathcal{U}}_0(t-t_\mathrm{c}, t_0-t_\mathrm{c})\hat{\Phi}(\phi)$ can then be written in terms of $\hat{\mathcal{U}}_0(t,t_0)$, with the diagonal operator $\hat{\Phi}(\phi)$ accounting for the pulse CEP. In the interval $[-T/2, T/2]$, the time evolution of $|\psi(t)\rangle = \hat{\mathcal{U}}_0(t,t_0)|\psi(t_0)\rangle$, depicted in Fig. 1(b), requires the solution of the Schrödinger equation (2) in the presence of the external pulse. In order to operatively describe this strong-field interaction, we introduce the *effective* initial and final states $|\psi^\mp\rangle = e^{i\hat{H}_0(\mp T/2)}|\psi(\mp T/2)\rangle$, represented in Fig. 1(b). We therefore define $\hat{U}(I) = e^{-i\hat{H}_0(-T/2)}\hat{\mathcal{U}}_0(T/2, -T/2)e^{i\hat{H}_0(T/2)}$ as the unique, intensity-dependent operator which connects $|\psi^+\rangle$ with $|\psi^-\rangle$ according to Eq. (1).

Endowed with an efficient way to quantify the action of strong ultrashort pulses, we can summarize our deterministic quantum-control scheme as follows. To prepare a system in a desired state $|\psi_\mathrm{d}\rangle$, we use the sequence of N_p pulses shown in Fig. 1(a), separated by delays $\bar{\tau}_m = t_{\mathrm{c},m+1} - t_{\mathrm{c},m}$ and leading the system to the state

$$|\psi_{N_\mathrm{p}}\rangle = \hat{\bar{U}}_{N_\mathrm{p}} \cdots \hat{V}(\bar{\tau}_m)\hat{\bar{U}}_m \cdots \hat{V}(\bar{\tau}_1)\hat{\bar{U}}_1|\psi_0\rangle. \tag{3}$$

Here, the action of the mth pulse, centered on $t_{\mathrm{c},m}$, is described by $\hat{\bar{U}}_m = \hat{\Phi}^\dagger(\phi_m)\hat{U}(I_m)\hat{\Phi}(\phi_m)$, with intensity I_m and CEP ϕ_m, $m \in \{1, \ldots, N_\mathrm{p}\}$.

As a final remark, we notice that, by using a Schrödinger-equation-based formalism with complex terms added to the energies of the system, coherences and populations are equally affected by dissipation, which renders the system open and the total population nonconserved. Here, however, we assume that the decay times $1/\gamma_i$ of the system are much larger than the femtosecond duration of the control pulses and of the pulse delays $\bar{\tau}_m$: the dynamics of the system *leading to the final state* $|\psi_{N_\mathrm{p}}\rangle$ in Eq. (3) are effectively insensitive to the details of

the dissipation process, justifying the use of a Schrödinger-like formalism in the initial sections of this paper. A density-matrix formalism is presented in Sec. VII.

III. TRANSIENT-ABSORPTION SPECTROSCOPY FOR MEASUREMENT-DRIVEN CONTROL

To exploit the advantages of a measurement-driven strategy without employing adaptive feedback, we utilize transient-absorption spectroscopy (TAS) to reconstruct $\hat{U}(I)$ in amplitude and phase, and use these extracted matrices for quantum-state control. TAS has been receiving increasing interest for studies of ultrafast dynamics [26–34]. The experimental setup is depicted in Fig. 2(a), with pump and probe pulses centered on $t_{c,pu} = 0$ and $t_{c,pr} = \tau$, respectively. In a pump-probe setup, the absorption spectrum $\mathcal{S}(\omega,\tau)$ of a transmitted weak probe pulse is observed for varying time delays τ, revealing the dynamics initiated by the intense pump pulse [35]. At the same time, recent experiments have employed a probe-pump scheme ($\tau < 0$), with the probe pulse generating a coherent superposition of quantum states which is subsequently nonlinearly excited by the strong pulse [29,36–38]. In this case, absorption spectral line shapes contain valuable information to quantify the strong-field dynamics induced by the pump pulse, albeit requiring schemes to extract information from complex time-dependent spectra. Characterizing strong-field interactions to reconstruct $\hat{U}(I)$ with TAS can be straightforwardly implemented experimentally, since the same intense pulse is used with varying time delays. This minimizes the number of experiments where pulse parameters need be precisely modified, in contrast to adaptive feedback, where pulse intensities, phases, and delays are simultaneously and controllably varied *at every iteration* to converge to the desired state.

For low densities, where propagation effects can be neglected and the pulses can be assumed to homogeneously control the sample, the time-delay-dependent spectra result from the system's single-particle dipole response,

$$\mathcal{S}_1(\omega,\tau) \propto -\omega \mathrm{Im}\left[\hat{\boldsymbol{e}}_z \cdot \int_{-\infty}^{\infty} \langle \hat{\boldsymbol{D}}^-(t,\tau)\rangle e^{-i\omega(t-\tau)} dt\right], \quad (4)$$

where $\langle \hat{\boldsymbol{D}}^-(t,\tau)\rangle = \mathrm{Tr}[\hat{\boldsymbol{D}}^- \hat{\rho}(t,\tau)]$ is the expectation value of the dipole-moment operator $\hat{\boldsymbol{D}}^- = \sum_{i>j} \boldsymbol{D}_{ij}|i\rangle\langle j|$, and the density matrix $\hat{\rho}(t,\tau) = \sum_{i,j} \rho_{ij}(t,\tau)|i\rangle\langle j|$ describes the time evolution of the system as a function of time delay. We assume a weak probe pulse, with full width at half maximum (FWHM) $T_{\mathrm{FWHM,pr}} = 15$ fs and intensity $I_{\mathrm{pr}} = 1 \times 10^8$ W/cm^2, and

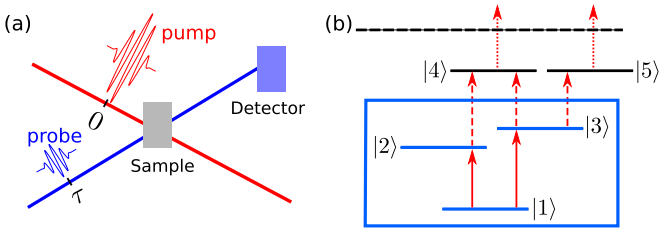

FIG. 2. (a) Transient-absorption-spectroscopy setup used to experimentally reconstruct strong-field interaction operators. (b) Level scheme used to model Rb atoms, aiming at the control of the V-type three-level scheme in the box.

pump pulses of duration $T_{\mathrm{FWHM,pu}} = 30$ fs and intensities I_{pu} varying between 0.1×10^{10} W/cm^2 and 5×10^{10} W/cm^2.

We apply our scheme to Rb atoms [21,39]. Specifically, we aim at controlling the V-type three-level system formed by the ground state $5s\,^2S_{1/2} \equiv |1\rangle$ and fine-structure-split excited states $5p\,^2P_{1/2} \equiv |2\rangle$ and $5p\,^2P_{3/2} \equiv |3\rangle$, with magnetic quantum numbers $M = \pm 1/2$ and transition energies $\omega_{21} = 1.56$ eV and $\omega_{31} = 1.59$ eV. The $E1$-allowed transitions $|1\rangle \rightarrow |k\rangle$, $k \in \{2,3\}$ [box in Fig. 2(b)] feature $\Delta M = 0$ and dipole-moment matrix elements $\boldsymbol{D}_{1k} = D_{1k}\hat{\boldsymbol{e}}_z$ [40]. For such a three-level model, in terms of the atomic coherences $\rho_{1k}(t,\tau)$, the absorption spectrum results from

$$\mathcal{S}_1(\omega,\tau) \propto -\omega \mathrm{Im}\left[\sum_{k=2}^{3} D_{1k}^* \int_{-\infty}^{\infty} \rho_{1k}(t,\tau) e^{-i\omega(t-\tau)} dt\right]. \quad (5)$$

For a system excited by the sole weak probe pulse, modeled as an effectively instantaneous interaction [Fig. 1(b)] and generating initial coherences $\rho_{1k,0}$, the ensuing decay of the coherences can be modeled as $\rho_{1k}(t,\tau) = \rho_{1k,0} e^{i\omega_{k1}(t-\tau)} e^{-(\gamma_k/2)(t-\tau)} \theta(t-\tau)$, with $\theta(x)$ being the Heaviside step function. Inserted into Eq. (5), this decay gives rise to stationary absorption lines, centered on the transition energies ω_{k1} and with Lorentzian shapes of width γ_k. In contrast, when an intense pump pulse is added, either preceding or following the probe pulse, the induced strong-field dynamics $\hat{\rho}(t,\tau)$ result in, e.g., asymmetric Fano-like absorption line shapes, which carry information about the action of the pump pulse on the atomic system. The fast oscillations of $\mathcal{S}_1(\omega,\tau)$ as a function of the time delay τ are averaged out in a noncollinear geometry [21] and cannot be discerned. This averaged time-delay-dependent spectrum is modeled via a convolution of the fast oscillating spectrum with a normalized Gaussian function $G(\tau,\Delta\tau)$ of width $\Delta\tau = 5 \times 2\pi/\omega_{\mathrm{L}}$ [21], thus obtaining

$$\mathcal{S}(\omega,\tau) = \langle \mathcal{S}_1(\omega,\tau)\rangle_\tau = \int_{-\infty}^{\infty} G(\tau-\tau',\Delta\tau)\,\mathcal{S}_1(\omega,\tau')d\tau'. \quad (6)$$

In the following, we will use decay rates $\gamma_2 = \gamma_3 = 1/(1500\ \mathrm{fs})$ to model experimental linewidths owing to, e.g., collision-induced and Doppler broadening. Radiative decay times of 27 ns and 25.7 ns, from the excited states $|2\rangle$ and $|3\rangle$, respectively, are more than four orders of magnitude larger than the duration of the femtosecond pulses used for our control scheme, and spontaneous decay can be neglected for our system. For femtosecond pulse delays $|\tau|$ and femtosecond pulse durations $T_{\mathrm{FWHM,pu}}$ and $T_{\mathrm{FWHM,pr}}$, much shorter than the decay times $1/\gamma_k$, the dynamics of the system *in between the two pulses*—i.e., for $0 < t < \tau$ in a pump-probe setup, or for $\tau < t < 0$ in a probe-pump setup—are effectively insensitive to the details of dissipation. In this time interval, dephasing is almost completely absent, and the system can be properly described in the same Schrödinger-like formalism presented in Sec. II, with the density matrix $\hat{\rho}(t,\tau) = |\psi(t,\tau)\rangle\langle\psi(t,\tau)|$ written in terms of the time-delay-dependent state vector $|\psi(t,\tau)\rangle = \sum_i c_i(t,\tau)|i\rangle$, such that $\rho_{ij} = c_i c_j^*$.

Dephasing becomes important only on much longer time scales. Our Schrödinger-equation-based approach, with a

complex-valued atomic-structure Hamiltonian, correctly describes the decay of the coherences in Eq. (5), thereby modeling the corresponding experimental linewidths. It does not provide the exact description of the evolution of the populations *following the interaction with the pump and probe pulses*, but this is not relevant for the modeling of the transient-absorption spectra and, thus, does not affect our operator-reconstruction method. In Secs. IV–VI, we will therefore present results based on a Schrödinger-like approach, with decay rates γ_k quantifying the slow dephasing of the system on time scales significantly exceeding $|\tau|$, $T_{\mathrm{FWHM,pu}}$, and $T_{\mathrm{FWHM,pr}}$. For completeness, and in particular to properly describe situations in which the details of dissipation are important on time scales comparable with time delays τ, we display how our results can be generalized to a more complex case requiring a density-matrix formulation in Sec. VII.

IV. RECONSTRUCTION OF STRONG-FIELD INTERACTION OPERATORS

In order to enable the extraction of strong-field interaction (SFI) operators from transient-absorption spectra, we take advantage of the same instantaneous-interaction model introduced in Eq. (1) and formally describe the system's dynamics in a pump-probe experiment in terms of the operators $\hat{U}_{\mathrm{pr}}$ and $\hat{U}_{\mathrm{pu}}(I)$. By means of Eqs. (5) and (6), we then derive an analytical fitting model to relate transient-absorption spectra to the matrix elements $U_{\mathrm{pu},ij}$ of the intensity-dependent pump-pulse operator $\hat{U}_{\mathrm{pu}}(I)$, and show how this model can be employed for the experimental reconstruction of $U_{\mathrm{pu},ij}$. For weak probe pulses, first-order perturbation theory is used to model $\hat{U}_{\mathrm{pr}}$, as shown in Appendix B, resulting in

$$\hat{U}_{\mathrm{pr}} \approx \begin{pmatrix} 1 & i\frac{\vartheta_2}{2} & i\frac{\vartheta_3}{2} \\ i\frac{\vartheta_2^*}{2} & 1 & 0 \\ i\frac{\vartheta_3^*}{2} & 0 & 1 \end{pmatrix}, \tag{7}$$

where the pulse areas $\vartheta_k = \int_{-T_{\mathrm{pr}}/2}^{T_{\mathrm{pr}}/2} D_{1k}\mathcal{E}_{0,\mathrm{pr}} f_{\mathrm{pr}}(t)dt, k \in \{2,3\}$, are defined in terms of duration and peak field strength of the probe pulse. In contrast, the matrix elements $U_{\mathrm{pu},ij}$ of the intensity-dependent pump-pulse operator $\hat{U}_{\mathrm{pu}}(I)$ are used as unknown fit parameters. In Sec. IV A, we provide a detailed derivation of the analytical fitting model $\mathcal{S}_{\mathrm{fit}}(\omega,\tau,U_{\mathrm{pu},ij})$ to interpret experimental spectra in a probe-pump setup, with the main result given in Eq. (13). In Sec. IV B, a model is similarly derived for a pump-probe setup, with the key formula presented in Eq. (18). Additional remarks for a full experimental extraction of interaction operators are provided in Sec. IV C. The Schrödinger-like formalism introduced in Secs. II and III is used throughout. A generalization of the scheme with a density-matrix description is presented in Sec. VII.

A. Probe-pump scheme

For a probe-pump scheme ($\tau < 0$), the weak probe pulse generates the initial excited state, which is nonperturbatively modified by the action of the second-arriving intense pump pulse. In terms of the operators $\hat{U}_{\mathrm{pr}}$ and $\hat{U}_{\mathrm{pu}}(I)$, modeling light-matter interactions as δ-like transformations, the effective evolution of the time-delay-dependent state $|\psi_{\mathrm{fit}}(t,\tau)\rangle = \sum_{i=1}^{3} c_{\mathrm{fit},i}(t,\tau)|i\rangle$ from the effective initial state $|\psi_0\rangle = |1\rangle$ is given by

$$|\psi_{\mathrm{fit}}(t,\tau)\rangle = \begin{cases} |\psi_0\rangle, & \text{if } t < \tau, \\ \hat{V}(t-\tau)\,\hat{U}_{\mathrm{pr}}\,|\psi_0\rangle, & \text{if } \tau < t < 0, \\ \hat{V}(t)\,\hat{U}_{\mathrm{pu}}(I)\,\hat{V}(-\tau)\,\hat{U}_{\mathrm{pr}}\,|\psi_0\rangle, & \text{if } t > 0. \end{cases} \tag{8}$$

We can analogously define the effective density-matrix elements $\rho_{\mathrm{fit},ij}(t,\tau) = c_{\mathrm{fit},i}(t,\tau)\,[c_{\mathrm{fit},j}(t,\tau)]^*$, in terms of the components $c_{\mathrm{fit},i}(t,\tau)$ of $|\psi_{\mathrm{fit}}(t,\tau)\rangle$. By inserting $\rho_{\mathrm{fit},ij}(t,\tau)$ into Eq. (5), an analytical interpretation model for the probe-pump spectrum is obtained as

$$\mathcal{S}_{1,\mathrm{fit}}(\omega,\tau,U_{\mathrm{pu},ij}) \propto -\omega\mathrm{Im}\left\{\sum_{k=2}^{3} D_{1k}^*\left[\int_{\tau}^{0}\rho_{\mathrm{fit},1k}(t,\tau)e^{-i\omega(t-\tau)}dt + \int_{0}^{\infty}\rho_{\mathrm{fit},1k}(t,\tau)e^{-i\omega(t-\tau)}dt\right]\right\}. \tag{9}$$

The first integral in Eq. (9) is equal to

$$\int_{\tau}^{0}\rho_{\mathrm{fit},1k}(t,\tau)e^{-i\omega(t-\tau)}dt = U_{\mathrm{pr},11}\,U_{\mathrm{pr},k1}^*\int_{\tau}^{0}V_{kk}^*(t-\tau)e^{-i\omega(t-\tau)}dt = -i\frac{\vartheta_k}{2}\frac{1-e^{i(\omega-\omega_{k1})\tau}e^{(\gamma_k/2)\tau}}{i(\omega-\omega_{k1})+\frac{\gamma_k}{2}}, \tag{10}$$

which, for $\omega \approx \omega_{k1}$, does not feature fast oscillations as a function of the time delay τ. The second integral in Eq. (9) is given by

$$\begin{aligned}\int_{0}^{\infty}\rho_{\mathrm{fit},1k}(t,\tau)e^{-i\omega(t-\tau)}dt &= \sum_{j,j'=1}^{3}U_{\mathrm{pu},1j}\,U_{\mathrm{pu},kj'}^*\,V_{jj}(-\tau)\,V_{j'j'}^*(-\tau)\,U_{\mathrm{pr},j1}\,U_{\mathrm{pr},j'1}^*\int_{0}^{\infty}V_{kk}^*(t)e^{-i\omega(t-\tau)}dt \\ &= \frac{1}{i(\omega-\omega_{k1})+\frac{\gamma_k}{2}}\sum_{j,j'=1}^{3}U_{\mathrm{pu},1j}\,U_{\mathrm{pu},kj'}^*[V_{jj}(-\tau)\,V_{j'j'}^*(-\tau)e^{i\omega\tau}]\,U_{\mathrm{pr},j1}\,U_{\mathrm{pr},j'1}^*.\end{aligned} \tag{11}$$

Firstly, all terms in the above sum depend upon nonvanishing elements of the probe-pulse operator $\hat{U}_{\mathrm{pr}}$ [Eq. (7)]. In a collinear geometry all terms in the above sum contribute to the resulting transient-absorption spectrum, which can be used to extract SFI matrix-element products such as $U_{\mathrm{pu},1j}\,U_{\mathrm{pu},kj'}$. In a noncollinear geometry, however, such as the one utilized in

Ref. [21], fast oscillating terms due to $[V_{jj}(-\tau)\,V^*_{j'j'}(-\tau)e^{i\omega\tau}]$ are averaged out and do not contribute to the resulting spectra. Equation (11) can be employed to recognize and eliminate all terms which, at $\omega \approx \omega_{k1}$, feature fast oscillations in τ. As a result, in terms of the two functions

$$A_2(\tau) = U_{\mathrm{pu},11}\,U^*_{\mathrm{pu},22} + U_{\mathrm{pu},11}\,U^*_{\mathrm{pu},23}\frac{\vartheta_3}{\vartheta_2}e^{-i\omega_{32}\tau}e^{[(\gamma_3-\gamma_2)/2]\tau},$$

$$A_3(\tau) = U_{\mathrm{pu},11}\,U^*_{\mathrm{pu},33} + U_{\mathrm{pu},11}\,U^*_{\mathrm{pu},32}\frac{\vartheta_2}{\vartheta_3}e^{i\omega_{32}\tau}\,e^{[(\gamma_2-\gamma_3)/2]\tau}, \tag{12}$$

average experimental spectra can be modeled by

$$\begin{aligned}\mathcal{S}_{\mathrm{fit}}(\omega,\tau,U_{\mathrm{pu},ij}) &= \langle \mathcal{S}_{1,\mathrm{fit}}(\omega,\tau,U_{\mathrm{pu},ij})\rangle_\tau \\ &\propto -\omega\mathrm{Im}\left(\sum_{k=2}^{3}\frac{-iD^*_{1k}\frac{\vartheta_k}{2}}{i(\omega-\omega_{k1})+\frac{\gamma_k}{2}}\{1+e^{i(\omega-\omega_{k1})\tau}e^{(\gamma_k/2)\tau}[A_k(\tau)-1]\}\right).\end{aligned} \tag{13}$$

The proportionality symbol $\propto$ stresses that these spectra depend on a density-dependent multiplication factor K, which we treat here as a fit parameter, along with the SFI matrix-element products $U_{\mathrm{pu},11}\,U^*_{\mathrm{pu},22}$, $U_{\mathrm{pu},11}\,U^*_{\mathrm{pu},33}$, $U_{\mathrm{pu},11}\,U^*_{\mathrm{pu},32}$, and $U_{\mathrm{pu},11}\,U^*_{\mathrm{pu},23}$.

B. Pump-probe scheme

For a pump-probe scheme ($\tau > 0$), in terms of the operators $\hat{U}_{\mathrm{pr}}$ and $\hat{U}_{\mathrm{pu}}(I)$, the effective evolution of the time-delay-dependent state $|\psi_{\mathrm{fit}}(t,\tau)\rangle$ from the effective initial state $|\psi_0\rangle = |1\rangle$ can be modeled as

$$|\psi_{\mathrm{fit}}(t,\tau)\rangle = \begin{cases}|\psi_0\rangle, & \text{if } t<0,\\ \hat{V}(t)\,\hat{U}_{\mathrm{pu}}(I)\,|\psi_0\rangle, & \text{if } 0<t<\tau,\\ \hat{V}(t-\tau)\,\hat{U}_{\mathrm{pr}}\,\hat{V}(\tau)\,\hat{U}_{\mathrm{pu}}(I)\,|\psi_0\rangle, & \text{if } t>\tau.\end{cases} \tag{14}$$

By including into Eq. (5) the effective evolution of the matrix elements $\rho_{\mathrm{fit},ij}(t,\tau)$ from Eq. (14), an analytical interpretation model for the pump-probe spectrum is derived, which can be split into the following sum:

$$\mathcal{S}_{1,\mathrm{fit}}(\omega,\tau,U_{\mathrm{pu},ij}) \propto -\omega\mathrm{Im}\left\{\sum_{k=2}^{3}D^*_{1k}\left[\int_0^\tau \rho_{\mathrm{fit},1k}(t,\tau)e^{-i\omega(t-\tau)}dt + \int_\tau^\infty \rho_{\mathrm{fit},1k}(t,\tau)e^{-i\omega(t-\tau)}dt\right]\right\}. \tag{15}$$

The first integral in Eq. (15) is equal to

$$\int_0^\tau \rho_{\mathrm{fit},1k}(t,\tau)e^{-i\omega(t-\tau)}dt = U_{\mathrm{pu},11}\,U^*_{\mathrm{pu},k1}\int_0^\tau V^*_{kk}(t)e^{-i\omega(t-\tau)}dt = U_{\mathrm{pu},11}\,U^*_{\mathrm{pu},k1}e^{i\omega\tau}\,\frac{1-e^{-i(\omega-\omega_{k1})\tau}e^{-(\gamma_k/2)\tau}}{i(\omega-\omega_{k1})+\frac{\gamma_k}{2}}. \tag{16}$$

As described in the case of the probe-pump scheme, the fast oscillations at frequencies $\omega \approx \omega_{k1}$ are averaged out in a noncollinear geometry, and this first integral does not contribute to the associated average absorption spectrum. The second integral in Eq. (15) is given by

$$\begin{aligned}\int_\tau^\infty \rho_{\mathrm{fit},1k}(t,\tau)e^{-i\omega(t-\tau)}dt &= \sum_{j,j'=1}^{3}U_{\mathrm{pr},1j}\,U^*_{\mathrm{pr},kj'}\,V_{jj}(\tau)\,V^*_{j'j'}(\tau)\,U_{\mathrm{pu},j1}\,U^*_{\mathrm{pu},j'1}\int_\tau^\infty V^*_{kk}(t-\tau)e^{-i\omega(t-\tau)}dt \\ &= \frac{1}{i(\omega-\omega_{k1})+\frac{\gamma_k}{2}}\sum_{j,j'=1}^{3}U_{\mathrm{pr},1j}\,U^*_{\mathrm{pr},kj'}[V_{jj}(\tau)\,V^*_{j'j'}(\tau)]U_{\mathrm{pu},j1}\,U^*_{\mathrm{pu},j'1}.\end{aligned} \tag{17}$$

By using Eq. (7) and removing fast oscillating terms due to $V_{jj}(\tau)\,V^*_{j'j'}(\tau)$, which would not appear in a noncollinear geometry, we conclude that

$$\begin{aligned}\mathcal{S}_{\mathrm{fit}}(\omega,\tau,U_{\mathrm{pu},ij}) &= \langle \mathcal{S}_{1,\mathrm{fit}}(\omega,\tau,U_{\mathrm{pu},ij})\rangle_\tau \\ &\propto -\omega\mathrm{Im}\left\{\frac{D^*_{12}}{i(\omega-\omega_{21})+\frac{\gamma_2}{2}}\left[\left(-i\frac{\vartheta_2}{2}|U_{\mathrm{pu},11}|^2 + i\frac{\vartheta_2}{2}|U_{\mathrm{pu},21}|^2e^{-\gamma_2\tau}\right) + i\frac{\vartheta_3}{2}\,U_{\mathrm{pu},31}\,U^*_{\mathrm{pu},21}e^{-i\omega_{32}\tau}e^{-[(\gamma_2+\gamma_3)/2]\tau}\right]\right. \\ &\quad \left. + \frac{D^*_{13}}{i(\omega-\omega_{31})+\frac{\gamma_3}{2}}\left[\left(-i\frac{\vartheta_3}{2}|U_{\mathrm{pu},11}|^2 + i\frac{\vartheta_3}{2}|U_{\mathrm{pu},31}|^2e^{-\gamma_3\tau}\right) + i\frac{\vartheta_2}{2}\,U_{\mathrm{pu},21}\,U^*_{\mathrm{pu},31}e^{i\omega_{32}\tau}e^{-[(\gamma_2+\gamma_3)/2]\tau}\right]\right\},\end{aligned} \tag{18}$$

which explicitly depends upon $|U_{\mathrm{pu},11}|^2$, $|U_{\mathrm{pu},22}|^2$, $|U_{\mathrm{pu},33}|^2$, and $(U_{\mathrm{pu},31}\,U^*_{\mathrm{pu},21})$. The same multiplication factor K should be used which was extracted from the probe-pump spectrum [see Eq. (13)].

C. Additional remarks

Summarizing the results from the above sections, one can fit probe-pump spectra to quantify $U_{\mathrm{pu},11}\,U^*_{\mathrm{pu},22}$, $U_{\mathrm{pu},11}\,U^*_{\mathrm{pu},33}$, $U_{\mathrm{pu},11}\,U^*_{\mathrm{pu},32}$, and $U_{\mathrm{pu},11}\,U^*_{\mathrm{pu},23}$, and the common multiplication factor K. Once K is known, it can be employed to fit pump-probe spectra, and thereby extract $|U_{\mathrm{pu},11}|^2$, $|U_{\mathrm{pu},21}|^2$, $|U_{\mathrm{pu},31}|^2$, and $(U_{\mathrm{pu},31}\,U^*_{\mathrm{pu},21})$.

All elements of the interaction operator $\hat{U}_{\mathrm{pu}}$ which can be retrieved from probe-pump spectra are inferred from product terms $U_{\mathrm{pu},11}U^*_{\mathrm{pu},ij}$, with $|U_{\mathrm{pu},11}|$ coming from pump-probe spectra. This has two consequences. Firstly, the phase β of $U_{\mathrm{pu},11} = |U_{\mathrm{pu},11}|e^{i\beta}$ cannot be accessed, resulting in SFI matrix elements

$$U_{\mathrm{pu},ij} = \frac{(U_{\mathrm{pu},11}U^*_{\mathrm{pu},ij})^*}{|U_{\mathrm{pu},11}|}e^{i\beta}, \tag{19}$$

known up to this common phase β. However, this is not a limitation, since it only implies that the final state can be measured and controlled up to a nonrelevant phase term, with access to the information about relevant relative phases. Secondly, when $|U_{\mathrm{pu},11}|$ is very close to 0, small uncertainties in its reconstructed value are amplified when the division in Eq. (19) is performed to retrieve the remaining matrix elements. For a certain range of pump-pulse intensities, we verified that this is indeed the main source of uncertainty in the extraction of $\hat{U}_{\mathrm{pu}}$, yet always below the relative level of 8%.

In a noncollinear geometry, the remaining pump-probe fit parameter $(U_{\mathrm{pu},31}\,U^*_{\mathrm{pu},21})$ can be used to quantify the relative phase $\arg(U_{\mathrm{pu},31}) - \arg(U_{\mathrm{pu},21})$, but not the absolute phases of $U_{\mathrm{pu},21}$ and $U_{\mathrm{pu},31}$—at least up to the same common phase β we introduced before. However, this can be easily circumvented by directly observing the absorption spectrum of a single intense pump pulse. The associated spectral lines are given by

$$\mathcal{S}_{\mathrm{fit}}(\omega, U_{\mathrm{pu},ij}) \propto -\omega \mathrm{Im}\left\{\mathcal{M} + \sum_{k=2}^{3} D^*_{1k}\int_0^\infty \rho_{\mathrm{fit},1k}(t)e^{-i\omega t}dt\right\}, \tag{20}$$

where $\mathcal{M}$ is a fit parameter modeling the broadband (and hence constant for small frequency intervals) Fourier transform of $\rho_{1k}(t)$ in the interval $[-T/2, T/2]$, i.e., in the presence of the pump pulse. The remaining integral

$$\begin{aligned}\int_0^\infty &\rho_{\mathrm{fit},1k}(t)e^{-i\omega t}dt \\ &= U_{\mathrm{pu},11}\,U^*_{\mathrm{pu},k1}\int_0^\infty e^{-i(\omega-\omega_{k1})t}e^{-(\gamma_k/2)t}dt \\ &= U_{\mathrm{pu},11}\,U^*_{\mathrm{pu},k1}\,\frac{1}{i(\omega-\omega_{k1})+\frac{\gamma_k}{2}}\end{aligned} \tag{21}$$

exploits the effective evolution of the system, given by

$$|\psi_{\mathrm{fit}}(t)\rangle = \begin{cases}|\psi_0\rangle, & \text{if } t < 0,\\ \hat{V}(t)\,\hat{U}_{\mathrm{pu}}(I)\,|\psi_0\rangle, & \text{if } t > 0.\end{cases} \tag{22}$$

Up to the same common phase β already mentioned above, this allows one to retrieve the phases of $U_{\mathrm{pu},21}$ and $U_{\mathrm{pu},31}$, complementing the amplitude information accessible by fitting pump-probe spectra.

Finally, in order to extract $U_{\mathrm{pu},12}$ and $U_{\mathrm{pu},13}$ in a noncollinear geometry, we exploit the fact that, when the envelope function $f(t) = f(-t)$ is a symmetric function of time, then the associated interaction operator $\hat{U}$ is a symmetric matrix, as shown in Appendix C, such that $U_{\mathrm{pu},1k} = U_{\mathrm{pu},k1}$. We stress that this is not a disadvantage of the operator-reconstruction scheme proposed here. As shown by Eq. (11), an independent extraction of $U_{\mathrm{pu},12}$ and $U_{\mathrm{pu},13}$, without additional assumptions on the envelope $f(t)$, is possible in a collinear geometry.

V. QUANTUM CONTROL GUIDED BY EXPERIMENTALLY CHARACTERIZED PULSES

The analytical fitting model presented in Sec. IV allows one to reconstruct the SFI operators $\hat{U}^{\mathrm{R}}(I)$ in amplitude and phase directly from experimental observables:

$$\left.\begin{matrix}\mathcal{S}_{\mathrm{exp}}(\omega,\tau)\\ \mathcal{S}_{\mathrm{fit}}(\omega,\tau,U_{\mathrm{pu},ij})\end{matrix}\right\} \xrightarrow[\text{fitting}]{} \text{Reconstructed operator } \hat{U}^{\mathrm{R}}. \tag{23}$$

Here, we solve the Schrödinger equation (2), with decay rates γ_k, and calculate the time evolution of the system interacting with delayed pump and probe pulses in a Schrödinger-like formalism. The details on the equations of motion are shown in Appendix A. We then use the obtained solution to simulate experimental spectra $\mathcal{S}_{\mathrm{exp}}(\omega,\tau)$ via Eqs. (5) and (6), for pump pulses of intensities varying between 0.1×10^{10} W/cm^2 and 5×10^{10} W/cm^2 and for the noncollinear geometry of Fig. 2(a) [21]. The effectiveness of the SFI reconstruction method is exemplified in Fig. 3(a), where we display the SFI matrix $\hat{U}^{\mathrm{R}}(I)$ extracted from the numerical simulation of absorption spectra $\mathcal{S}(\omega,\tau)$, for a pump intensity of $I = 3.3\times10^{10}$ W/cm^2. The same reconstruction scheme could

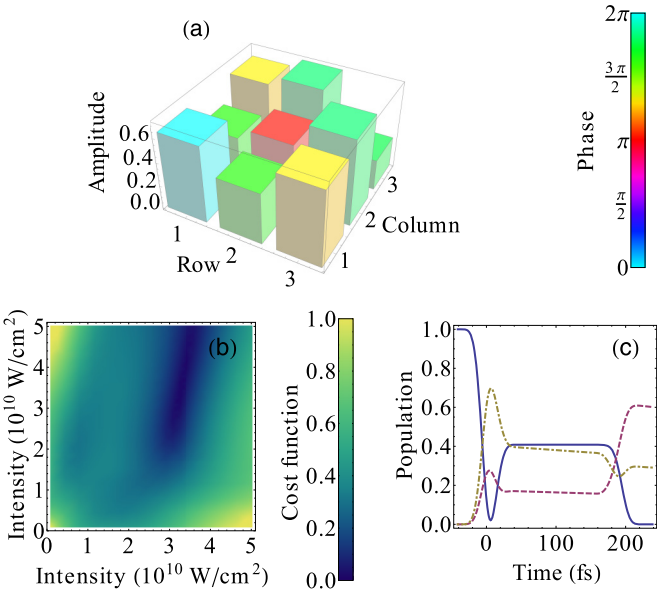

FIG. 3. (a) Reconstructed SFI operator $\hat{U}^{\mathrm{R}}(I)$ for $I = 3.3\times10^{10}$ W/cm^2, with bar heights (colors) exhibiting matrix-element amplitudes (phases). (b), (c) Two-pulse scheme implemented for $I_1 = 3.3\times10^{10}$ W/cm^2, $I_2 = 3.6\times10^{10}$ W/cm^2, $\bar{\tau} = 198$ fs, and $\bar{\phi} = 1.88$ rad, with (b) a section of the control landscape as a function of I_1 and I_2, for fixed $\bar{\tau}$ and $\bar{\phi}$ and (c) the corresponding evolution of the populations of state $|1\rangle$ (blue, continuous), $|2\rangle$ (purple, dashed), and $|3\rangle$ (yellow, dot-dashed), with a reached final state $|\psi_{\mathrm{r}}\rangle = \sum_{i=1}^{3} c_{\mathrm{r},i}|i\rangle$ featuring $|c_{\mathrm{r},2}|^2/|c_{\mathrm{r},3}|^2 = 2.07$ and $c_{\mathrm{r},1} = 0.00$.

be implemented in an experiment, enabling access to strong-field light-matter interactions without requiring knowledge of pump-pulse intensities or the system's dynamics.

Once SFI operators are reconstructed as a function of pulse intensities, these are employed to implement our deterministic control method from Eq. (3). In the following, we focus on a two-pulse scheme, and use reconstructed SFI operators to optimize time separation $\bar{\tau}$, intensities I_m, and CEPs ϕ_m, $m \in \{1,2\}$, to control the populations of the final state $|\psi_2\rangle$. This yields a predicted final state

$$|\psi_{\rm p}\rangle = \sum_{i=1}^{3} c_{{\rm p},i}|i\rangle = \hat{U}^{\rm R}(I_2)\hat{\Phi}(\bar{\phi})\hat{W}(\bar{\tau})\hat{U}^{\rm R}(I_1)\,|1\rangle, \qquad (24)$$

where we neglect phase terms not influencing the final populations, and introduce the total phase $\bar{\phi} = \phi_2 - \phi_1 - \omega_{\rm L}\bar{\tau}$, the CEP operator $\hat{\Phi}(\phi) = {\rm diag}(1, e^{i\phi}, e^{i\phi})$, and the slowly oscillating operator $\hat{W}(\bar{\tau}) = {\rm diag}(1, e^{-[\gamma_2/2+i(\omega_{21}-\omega_{\rm L})]\bar{\tau}}, e^{-[\gamma_3/2+i(\omega_{31}-\omega_{\rm L})]\bar{\tau}})$.

In order to show how coherently controlled dynamics can be interpreted in terms of experimentally reconstructed SFI operators, in Fig. 3 we present results for a sequence of two strong pulses aiming at the desired state $|\psi_{\rm d}\rangle = \sum_{i=1}^{3} c_{{\rm d},i}|i\rangle$, of amplitudes $(c_{{\rm d},1}, c_{{\rm d},2}, c_{{\rm d},3}) = Ae^{i\gamma}\,(0, \sqrt{2/3}, e^{i\delta}\sqrt{1/3})$, such that the ground state is completely depopulated, while the excited state $|2\rangle$ is twice as much populated as $|3\rangle$, despite a less favorable coupling to the ground state. The total final population A^2 and the phases γ and δ are free parameters. Optimal pulse properties are determined via minimization of the cost function [1]

$$g(I_1, I_2, \bar{\tau}, \bar{\phi}) = \sqrt{\sum_{i=1}^{3} \left| |c_{{\rm d},i}|^2 - |c_{{\rm p},i}|^2 \right|^2}, \qquad (25)$$

calculated for a discrete set of parameters and ensuring that $|\langle\psi_{\rm d}|\psi_{\rm d}\rangle|^2 = |\langle\psi_{\rm p}|\psi_{\rm p}\rangle|^2 = A^2$.

Techniques from quantum optimal control theory have been developed to analyze quantum-control landscapes [1] and determine how a desired state can be optimally reached with pulse shaping. Similar methods could be implemented in our case in order to identify the volume in the Hilbert space spanned by the vector states $|\psi_{\rm p}\rangle$ in Eq. (24) and whether the desired final state $|\psi_{\rm d}\rangle$ lies in this volume. Thereby, a sequence of pulses can be optimally designed in order to minimize the cost function $g(I_1, I_2, \bar{\tau}, \bar{\phi})$ and, thus, guide the system to $|\psi_{\rm d}\rangle$. In contrast to quantum optimal control theory, however, deterministic strong-field control enables this numerical optimization based on experimentally reconstructed SFI operators.

A section of the control landscape [1], associated with global minima of the cost function g, is displayed in Fig. 3(b), confirming that it is a smooth function of its parameters, and small uncertainties in the pulse intensities do not lead to final states significantly differing from those expected. Figure 3(c) shows the resulting dynamics of the system [Eq. (2)], when excited with the sequence of pulses determined via minimization of g, exhibiting very good agreement with the desired final state. The displayed dynamics could be directly inferred from the reconstructed SFI operators. The state reached after the first intense pulse in Fig. 3(c) is completely encoded in the matrix elements plotted in Fig. 3(a), such that deterministic strong-field control provides an experiment-based visualization of the building blocks exploited by optimal control to reach a desired state. Rabi oscillations induced by strong ultrashort pulses are apparent in Fig. 3(c), but knowledge of their explicit time dependence is not necessary to control the reached final state. Although we focus on the control of final populations, this nevertheless requires phase knowledge of $\hat{U}^{\rm R}(I)$. In addition, $\hat{\Phi}(\bar{\phi})$ and $\hat{V}(\bar{\tau})$ allow one to independently control the phase acquired by the two excited states $|2\rangle$ and $|3\rangle$ in the time delay $\bar{\tau}$ between the two pulses [2].

VI. PERFORMANCES OF THE SCHEME IN THE PRESENCE OF INCOMPLETE MODELING

To verify the precision of the scheme, in Figs. 4(a) and 4(b) we display final populations reached by the three-level system when integrating Eq. (2) for the sequences of pulses determined through the minimization of Eq. (25). The extracted SFI operators have an intrinsic uncertainty, and we therefore display results averaged among the first N best sets of optimization parameters (with standard deviation) as a function of N. Very good control performances are exhibited: complete depopulation of the ground state is reached [Fig. 4(a)], and the mean value of the ratio $|c_2/c_3|^2$ is equal to 2 for the first best sets of optimization parameters, with relative uncertainty of $\sim$3% [Fig. 4(b)].

Finally, we test our scheme in a realistic scenario, characterized by the presence of incomplete modeling or perturbations. To derive $\mathcal{S}_{\rm fit}(\omega, \tau, U_{{\rm pu},ij})$ from Eq. (6), basic knowledge of the atomic transitions responsible for the

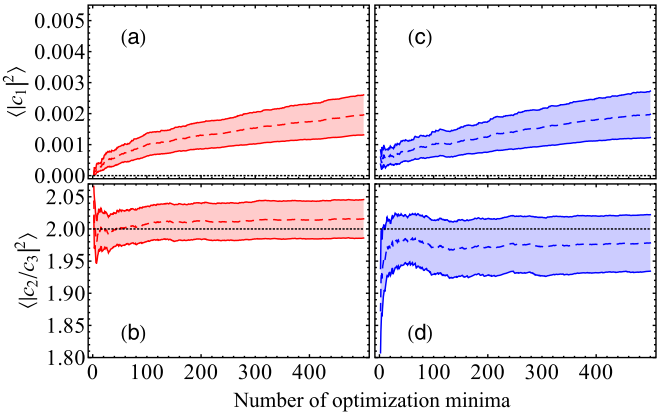

FIG. 4. [(a),(c)] Reached ground-state population and [(b),(d)] ratio of the populations of the two excited states $|2\rangle$ and $|3\rangle$, averaged over the N best sets of optimization pulse parameters $\{I_1, I_2, \bar{\tau}, \bar{\phi}\}$, as a function of N. Mean values are displayed as dashed lines; the surrounding regions (bounded by continuous lines) have an amplitude given by the corresponding standard deviation. Desired final population and ratios are exhibited by black, dotted lines. Reached final populations and ratios are calculated for [(a),(b)] a three-level-only system and [(c),(d)] a five-level system. The best optimization parameters are obtained via minimization of the cost function (25), calculated with SFI operators $\hat{U}^{\rm R}(I)$ reconstructed from transient-absorption spectra numerically simulated for [(a),(b)] a three-level and [(c),(d)] a five-level model.

absorption lines appearing in the spectrum is necessary. A robust control scheme should enable the manipulation of the states of interest also when additional, moderately contributing levels are present, which may not be known or experimentally discernible. As an example, we employ the analytical fitting model $\mathcal{S}_{\rm fit}(\omega,\tau,U_{{\rm pu},ij})$ to extract 3×3 SFI operators $\hat{U}^{\rm R}$ from transient-absorption spectra in Rb atoms, stemming from the complete numerical simulation of the dynamics of the five-level system displayed in Fig. 2(b). The $E1$-allowed transitions $|2\rangle \rightarrow |4\rangle$, $|3\rangle \rightarrow |4\rangle$, and $|3\rangle \rightarrow |5\rangle$, with $\Delta M = 0$, with transition energies $\omega_{42} = 1.63$ eV and $\omega_{53} = 1.60$ eV, are resonantly excited by the optical pulses, albeit more weakly than the $|1\rangle \rightarrow |k\rangle$ transitions, $k \in \{2,3\}$, owing to smaller dipole-moment matrix elements $\boldsymbol{D}_{kl} = D_{kl}\hat{\boldsymbol{e}}_z$, $l \in \{4,5\}$ [41,42]. To ensure that this resonant coupling contributes moderately, we assume large linewidths γ_4 and γ_5, here set equal to $1/(100$ fs) [43], such that only the two lines associated with the $|1\rangle \rightarrow |k\rangle$ transitions can be clearly distinguished in the absorption spectra. Photoionization in the presence of an optical pulse is also accounted for [44]. SFI operators $\hat{U}^{\rm R}(I)$ are extracted from these numerically calculated spectra, and used to control the three-level system in the box of Fig. 2(b) via minimization of the cost function g. The very good performances displayed in Figs. 4(c) and 4(d) confirm that the method is robust and only marginally influenced by additional levels not accounted for explicitly in $\mathcal{S}_{\rm fit}(\omega,\tau,U_{{\rm pu},ij})$. Furthermore, in contrast to methods based exclusively on theory, maximal information on the strong-field interaction is extracted from the experimental spectra, including the background effect of unknown additional levels on the SFI operators $\hat{U}^{\rm R}(I)$ of interest.

Adding chirp may increase the probability to populate the excited states $|4\rangle$ and $|5\rangle$ [45] and would render it necessary to extract the SFI operator associated with the full five-level system. This would require a full analytical fitting model to interpret transient-absorption spectra from the associated five-level system as a function of the pump-pulse intensity and chirp. However, it would enable more general control schemes, based on sequences of intense chirped pulses, in order to create desired final states which are a superposition of all five levels.

VII. DETERMINISTIC STRONG-FIELD QUANTUM CONTROL WITH DENSITY-MATRIX INTERACTION OPERATORS

Our deterministic strong-field control method has been thus far discussed in a Schrödinger-like formalism, in terms of state vectors $|\psi\rangle$ and the associated SFI operators $\hat{U}(I)$ defined in Sec. II. The equations of motion (Appendix A), assuming a decay-rate model with a complex-valued atomic-structure Hamiltonian, were used to simulate transient-absorption spectra, and the analytical fitting model developed in Sec. IV was used in Secs. V and VI to reconstruct SFI operators $\hat{U}(I)$. For our implementation with Rb atoms, this is a proper treatment, in the light of the very different time scales in which the strong-field dynamics and the relaxation of the system take place. For more general cases, however, a density-matrix formulation of our operator-reconstruction and quantum-control scheme is possible, as we show in the following. In this section, we will focus on the case of a three-level system, although the equations can be easily generalized to higher numbers of levels if necessary.

A. Density-matrix interaction operators

We describe the system in terms of a 3×3 density matrix $\hat{\rho}(t) = \sum_{i,j}\rho_{ij}(t)|i\rangle\langle j|$, with a diagonal element $\rho_{ii}(t)$ associated with the population of the ith level, and off-diagonal matrix elements for the atomic coherences. A density-matrix formulation may be necessary, e.g., to explicitly account for the spontaneous decay of the two excited levels $|2\rangle$ and $|3\rangle$ into the ground state $|1\rangle$, at rates given by γ_{22} and γ_{33}, respectively. Similarly, it is necessary to account for decoherence processes differently affecting the atomic coherences ρ_{12}, ρ_{13}, and ρ_{23}, than the populations ρ_{22} and ρ_{33}. In this section, we introduce the decoherence rates γ_{21}, γ_{31}, and γ_{23}, to quantify the dephasing of ρ_{12}, ρ_{13}, and ρ_{23}, respectively. The time evolution of $\hat{\rho}(t)$ is determined by the solution of the master equation

$$\frac{d\hat{\rho}(t)}{dt} = i[\hat{\rho}(t),\hat{H}_0+\hat{H}_{\rm int}]+\mathcal{L}[\hat{\rho}(t)], \quad \hat{\rho}(t_0)=\hat{\rho}_0=|1\rangle\langle 1|, \tag{26}$$

with the atomic-structure Hamiltonian now given by $\hat{H}_0 = \sum\omega_i|i\rangle\langle i|$, the same $E1$ light-matter interaction Hamiltonian $\hat{H}_{\rm int}$ introduced in Sec. II, and the superoperator $\mathcal{L}[\hat{\rho}(t)]$ describing dissipation. The explicit form of the set of differential equations

$$\frac{d\rho_{ij}(t)}{dt} = \sum_{i'j'}\mathfrak{M}_{ij,i'j'}(t)\rho_{i'j'}(t), \tag{27}$$

satisfied by the elements $\rho_{ij}(t)$ of the density matrix $\hat{\rho}(t)$ in terms of the elements $\mathfrak{M}_{ij,i'j'}(t)$ of the operator $\hat{\mathfrak{M}}(t)$, $i,j,i',j' \in \{1,2,3\}$, is given in detail in Appendix D. In analogy to the discussion provided in Sec. II, the state $\hat{\rho}(t)$ at time t can be related to the state $\hat{\rho}(t_0)$ at time t_0 via the evolution operator $\hat{\mathfrak{U}}(t,t_0)$, such that $\rho_{ij}(t) = \sum_{i'j'}\mathfrak{U}_{ij,i'j'}(t,t_0)\rho_{i'j'}(t_0)$, where

$$\begin{aligned}\frac{d\mathfrak{U}_{ij,i'j'}(t,t_0)}{dt} &= \sum_{i''j''}\mathfrak{M}_{ij,i''j''}(t)\mathfrak{U}_{i''j'',i'j'}(t,t_0),\\ \mathfrak{U}_{ij,i'j'}(t_0,t_0) &= \delta_{ii'}\delta_{jj'}.\end{aligned} \tag{28}$$

In order to highlight the difference between the present density-matrix formulation and the Schrödinger-like formalism used in the previous sections, we write explicitly the equations of motion (27) satisfied by the elements of the density matrix in the absence of external fields:

$$\begin{aligned}\frac{d\rho_{11}}{dt} &= \gamma_{22}\rho_{22}+\gamma_{33}\rho_{33},\\ \frac{d\rho_{kk}}{dt} &= -\gamma_{kk}\rho_{kk},\\ \frac{d\rho_{1k}}{dt} &= -\gamma_{k1}\rho_{1k}+i\omega_{k1}\rho_{1k},\\ \frac{d\rho_{23}}{dt} &= -\gamma_{23}\rho_{23}+i\omega_{32}\rho_{23},\end{aligned} \tag{29}$$

with $k \in \{2,3\}$ and $\rho_{ij} = \rho^*_{ji}$. Here, population decay from the excited states back to the ground state is explicitly

accounted for, ensuring that the total population $\rho_{11}(t)+\rho_{22}(t)+\rho_{33}(t)=1$ is conserved; furthermore, we employ different decay rates for coherences and populations. From the above equations, the free evolution of the system is given by

$$\begin{aligned}\rho_{11}(t)&=\rho_{11}(t_0)+\rho_{22}(t_0)(1-e^{-\gamma_{22}(t-t_0)})\\&\quad+\rho_{33}(t_0)(1-e^{-\gamma_{33}(t-t_0)}),\\\rho_{kk}(t)&=\rho_{kk}(t_0)e^{-\gamma_{kk}(t-t_0)},\\\rho_{1k}(t)&=\rho_{1k}(t_0)e^{-\gamma_{k1}(t-t_0)}e^{i\omega_{k1}(t-t_0)},\\\rho_{23}(t)&=\rho_{23}(t_0)e^{-\gamma_{23}(t-t_0)}e^{i\omega_{32}(t-t_0)}.\end{aligned}\tag{30}$$

The coefficients in the above set of equations define the elements of the operator $\hat{\mathbf{V}}(t)$, which can be used to describe the free evolution of the density matrix as $\rho_{ij}(t)=\sum_{i'j'}\mathbf{V}_{ij,i'j'}(t-t_0)\rho_{i'j'}(t_0)$.

In analogy to the derivation of the SFI operators $\hat{U}(I)$ in Sec. II, also in this case we focus on pulses centered on $t_c=0$ and with vanishing CEP, associated with the evolution operator $\hat{\mathfrak{U}}_0(t,t_0)$. The generic evolution operator $\hat{\mathfrak{U}}(t,t_0)$ then has components $\mathfrak{U}_{ij,i'j'}(t,t_0)=\mathbf{\Phi}^*_{ij,ij}(\phi)\mathfrak{U}_{0;ij,i'j'}(t-t_c,t_0-t_c)\mathbf{\Phi}_{i'j',i'j'}(\phi)$, where the operator $\hat{\mathbf{\Phi}}(\phi)$ accounts for the pulse CEP and its components $\mathbf{\Phi}_{ij,i'j'}(\phi)=\Phi_{ii'}(\phi)\Phi^*_{jj'}(\phi)$ are defined in terms of the diagonal operator $\hat{\Phi}(\phi)=\sum_i\Phi_{ii}(\phi)|i\rangle\langle i|$ introduced in Sec. II. For a pulse nonvanishing in the interval $[-T/2,T/2]$, we can then introduce *effective* initial and final density matrices $\rho^{\mp}_{ij}=\sum_{i'j'}\mathbf{V}_{ij,i'j'}(\pm T/2)\rho_{i'j'}(\mp T/2)$, and the unique density-matrix interaction operator $\hat{\mathbf{U}}(I)$ connecting them,

$$\rho^{+}_{ij}=\sum_{i'j'}\mathbf{U}_{ij,i'j'}(I)\rho^{-}_{i'j'},\tag{31}$$

whose components are given by $\mathbf{U}_{ij,i'j'}(I)=\sum_{i''j''}\sum_{i'''j'''}[\mathbf{V}_{ij,i''j''}(-T/2)\mathfrak{U}_{0;i''j'',i'''j'''}(T/2,-T/2)\mathbf{V}_{i'''j''',i'j'}(-T/2)]$. The deterministic quantum-control method outlined in Eq. (3) in a Schrödinger-like formalism can then be generalized to the case in which a density-matrix description is required. For example, for two control pulses of intensities I_1 and I_2, CEPs ϕ_1 and ϕ_2, and separated by a time delay $\bar{\tau}$, the state reached by the system is described by a density matrix $\hat{\rho}_2$ of components

$$\rho_{2;ij}=\sum_{i'j'}\sum_{i''j''}\sum_{i'''j'''}\tilde{\mathbf{U}}_{2;ij,i'j'}\mathbf{V}_{i'j',i''j''}(\bar{\tau})\tilde{\mathbf{U}}_{1;i''j'',i'''j'''}\rho_{0;i'''j'''},\tag{32}$$

with the initial state given by the density matrix $\hat{\rho}_0=|1\rangle\langle 1|$ and the components $\tilde{\mathbf{U}}_{m;ij,i'j'}=\mathbf{\Phi}^*_{ij,ij}(\phi_m)\mathbf{U}_{ij,i'j'}(I_m)\mathbf{\Phi}_{i'j',i'j'}(\phi_m)$ of the mth-pulse operator $\hat{\tilde{\mathbf{U}}}_m$, $m\in\{1,2\}$, accounting for the effect of the CEP of the associated pulse.

B. Reconstruction of density-matrix strong-field interaction operators

In order to extract density-matrix SFI (DM-SFI) operators from TAS, an analytical fitting model has to be developed, relating the spectra given by Eqs. (5) and (6) to the operators $\hat{\mathbf{U}}_{pu}(I)$ and $\hat{\mathbf{U}}_{pr}$, associated with a pump pulse of intensity I and a probe pulse, respectively.

For ultrashort pulses, acting on a time scale much shorter than the time scale of the decay processes, it is valid to assume that $\hat{\mathbf{U}}=\hat{U}\otimes\hat{U}^*$, i.e., $\mathbf{U}_{ij,i'j'}=U_{ii'}U^*_{jj'}$, for both pump and probe pulses. This assumption does not affect the numerical integration of the equations of motion (27) and the simulation of transient-absorption spectra in Sec. VII C. In contrast to Sec. IV and Appendix A, however, here we fully account for the details of the relaxation of the system during its free evolution, modeling the dynamics in between pump and probe pulses in terms of the free-evolution operator $\hat{\mathbf{V}}(t)$. A similar approach can be used to model quantum systems also in the presence of a more structured reservoir, provided that the free evolution of the system is known and can be used to define the operator $\hat{\mathbf{V}}(t)$. This will be exemplified in Sec. VII C, where spectra are numerically simulated based on the evolution of the density matrix, and used to extract the associated DM-SFI operators.

For a TAS experiment in a probe-pump setup, we can describe the effective evolution of the time-delay-dependent density matrix $\hat{\rho}_{fit}(t,\tau)$ from the effective initial state $\hat{\rho}_0=|1\rangle\langle 1|$ as

$$\rho_{\mathrm{fit};ij}(t,\tau)=\begin{cases}\rho_{0;ij} & \text{if } t<\tau,\\ \mathbf{V}_{ij,i'j'}(t-\tau)\,\mathbf{U}_{\mathrm{pr};i'j',i''j''}\,\rho_{0;i''j''} & \text{if } \tau<t<0,\\ \mathbf{V}_{ij,kl}(t)\,\mathbf{U}_{\mathrm{pu};kl,k'l'}(I)\,\mathbf{V}_{k'l',i'j'}(-\tau)\,\mathbf{U}_{\mathrm{pr};i'j',i''j''}\,\rho_{0;i''j''} & \text{if } t>0,\end{cases}\tag{33}$$

where summation over repeated indices is implicit. By inserting $\rho_{\mathrm{fit},ij}(t,\tau)$ into Eq. (5), an analytical interpretation model for the probe-pump spectrum is obtained consisting also in this case of two integrals. The first integral reads

$$\int_{\tau}^{0}\rho_{\mathrm{fit},1k}(t,\tau)e^{-i\omega(t-\tau)}dt=\int_{\tau}^{0}\sum_{i,j=1}^{3}\mathbf{V}_{1k,ij}(t-\tau)\,\mathbf{U}_{\mathrm{pr};ij,11}e^{-i\omega(t-\tau)}dt=-i\frac{\vartheta_k}{2}\frac{1-e^{i(\omega-\omega_{k1})\tau}e^{\gamma_{k1}\tau}}{i(\omega-\omega_{k1})+\gamma_{k1}},\tag{34}$$

where we have used the fact that $\mathbf{V}_{1k,ij}(t)=e^{-\gamma_{k1}t}e^{i\omega_{k1}t}\delta_{1i}\delta_{kj}$ [Eq. (D9)]. The second integral is similarly given by

$$\begin{aligned}\int_{0}^{\infty}\rho_{\mathrm{fit},1k}(t,\tau)e^{-i\omega(t-\tau)}dt&=\sum_{i,j=1}^{3}\sum_{i',j'=1}^{3}\sum_{i'',j''=1}^{3}\mathbf{U}_{\mathrm{pu};ij,i'j'}\,\mathbf{V}_{i'j',i''j''}(-\tau)\,\mathbf{U}_{\mathrm{pr},i''j'',11}\int_{0}^{\infty}\mathbf{V}_{1k,ij}(t)e^{-i\omega(t-\tau)}dt\\&=\frac{1}{i(\omega-\omega_{k1})+\gamma_{k1}}\sum_{i',j'=1}^{3}\sum_{i'',j''=1}^{3}U_{\mathrm{pu},1i'}U^*_{\mathrm{pu},kj'}[\mathbf{V}_{i'j',i''j''}(-\tau)e^{i\omega\tau}]\,U_{\mathrm{pr},i''1}U^*_{\mathrm{pr},j''1}.\end{aligned}\tag{35}$$

By including explicitly the values of $\mathbf{V}_{i'j',i''j''}(-\tau)$ from Eq. (D9), one obtains an equation in which, in contrast to Eq. (11), different decay rates for coherences and populations are present and additional terms appear due to the spontaneous decay from the excited states to the ground state. In order to model spectra from a noncollinear geometry, fast oscillating terms due to $[\mathbf{V}_{i'j',i''j''}(-\tau)e^{i\omega\tau}]$ can be eliminated, resulting in the average spectrum

$$\langle \mathcal{S}_{\mathrm{fit}}(\omega,\tau,U_{\mathrm{pu},ij})\rangle_\tau \propto -\omega \mathrm{Im}\left\{\sum_{k=2}^{3} D^*_{1k}\frac{1}{i(\omega-\omega_{k1})+\gamma_{k1}}\left[-i\frac{\vartheta_k}{2}(1-e^{i(\omega-\omega_{k1})\tau}e^{\gamma_{k1}\tau})\right.\right.$$
$$\left.\left.-i\frac{\vartheta_2}{2}U_{\mathrm{pu},11}\,U^*_{\mathrm{pu},k2}e^{i(\omega-\omega_{21})\tau}e^{\gamma_{21}\tau}-i\frac{\vartheta_3}{2}U_{\mathrm{pu},11}U^*_{\mathrm{pu},k3}e^{i(\omega-\omega_{31})\tau}e^{\gamma_{31}\tau}\right]\right\}. \quad (36)$$

In a pump-probe setup, the same formalism can be used, resulting in an effective evolution given by

$$\rho_{\mathrm{fit};ij}(t,\tau)=\begin{cases}\rho_{0;ij} & \text{if } t<0,\\ \mathbf{V}_{ij,i'j'}(t)\,\mathbf{U}_{\mathrm{pu};i'j',i''j''}(I)\,\rho_{0;i''j''} & \text{if } 0<t<\tau,\\ \mathbf{V}_{ij,kl}(t-\tau)\,\mathbf{U}_{\mathrm{pr};kl,k'l'}\,\mathbf{V}_{k'l',i'j'}(\tau)\,\mathbf{U}_{\mathrm{pu};i'j',i''j''}(I)\,\rho_{0;i''j''} & \text{if } t>\tau,\end{cases} \quad (37)$$

where, also in this case, summation over repeated indices is implicit. By following the same procedure outlined for the probe-pump case, and after removing the fast oscillating terms, one obtains the average spectrum given by

$$\langle \mathcal{S}_{\mathrm{fit}}(\omega,\tau,U_{\mathrm{pu},ij})\rangle_\tau \propto -\omega \mathrm{Im}\left\{\frac{D^*_{12}}{i(\omega-\omega_{21})+\gamma_{21}}\left[\left(-i\frac{\vartheta_2}{2}|U_{\mathrm{pu},11}|^2+i\frac{\vartheta_2}{2}|U_{\mathrm{pu},21}|^2(2e^{-\gamma_{22}\tau}-1)+i\frac{\vartheta_2}{2}|U_{\mathrm{pu},31}|^2(e^{-\gamma_{33}\tau}-1)\right)\right.\right.$$
$$\left.+i\frac{\vartheta_3}{2}\,U_{\mathrm{pu},31}\,U^*_{\mathrm{pu},21}e^{-i\omega_{32}\tau}e^{-\gamma_{23}\tau}\right]+\frac{D^*_{13}}{i(\omega-\omega_{31})+\gamma_{31}}\left[\left(-i\frac{\vartheta_3}{2}|U_{\mathrm{pu},11}|^2+i\frac{\vartheta_3}{2}|U_{\mathrm{pu},31}|^2\,(2e^{-\gamma_{33}\tau}-1)\right.\right.$$
$$\left.\left.+i\frac{\vartheta_3}{2}|U_{\mathrm{pu},21}|^2\,(e^{-\gamma_{22}\tau}-1)\right)+i\frac{\vartheta_2}{2}U_{\mathrm{pu},21}\,U^*_{\mathrm{pu},31}e^{i\omega_{32}\tau}e^{-\gamma_{23}\tau}\right]\right\}. \quad (38)$$

Also in this case, in contrast to Eq. (18), we notice different decay rates and the presence of additional terms to account for the decay into the ground state $|1\rangle$. The above expression can be further simplified by taking into account that

$$|U_{\mathrm{pu},11}|^2=1-|U_{\mathrm{pu},21}|^2-|U_{\mathrm{pu},31}|^2 \quad (39)$$

for a system which is not open and whose total population is conserved.

Finally, the absorption spectrum of a single intense pulse can be modeled as

$$\mathcal{S}_{\mathrm{fit}}(\omega,U_{\mathrm{pu},ij})$$
$$\propto -\omega \mathrm{Im}\left\{\mathcal{M}+\sum_{k=2}^{3}\frac{D^*_{1k}}{i(\omega-\omega_{k1})+\gamma_{k1}}U_{\mathrm{pu},11}U^*_{\mathrm{pu},k1}\right\}, \quad (40)$$

which generalizes Eq. (20) to the present case employing a density-matrix formalism.

In conclusion, analytical fitting models are developed to express transient-absorption spectra in terms of the elements of the density-matrix interaction operator $\hat{\mathbf{U}}_{\mathrm{pu}}(I)$. We assume that pump and probe operators are well approximated by $\mathbf{U}_{\mathrm{pu};ij,i'j'}(I)=U_{\mathrm{pu},ii'}(I)U^*_{\mathrm{pu},jj'}(I)$ and $\mathbf{U}_{\mathrm{pr};ij,i'j'}=U_{\mathrm{pr},ii'}U^*_{\mathrm{pr},jj'}$, which is valid for femtosecond pump and probe pulses much shorter than the decay time of the system. However, the relaxation of the system during its free decay in between the two pulses is modeled in terms of the free-evolution operator $\hat{\mathbf{V}}(t)\neq\hat{V}(t)\otimes\hat{V}^*(t)$, fully accounting for the different rates at which populations and coherences decay, and for the conservation of the total population. By employing Eq. (39) to ensure population conservation during the interaction with a pump pulse, and by further taking advantage of the symmetry properties of $\hat{\mathbf{U}}(I)$ discussed in Appendix C, the analytical models presented in this section can be employed to fit experimental spectra and, thereby, fully reconstruct DM-SFI operators $\hat{\mathbf{U}}^{\mathrm{R}}(I)$ in those cases in which a density-matrix description of the free evolution of the system is required.

C. Density-matrix quantum control based on strong-field interaction operators

The analytical fitting models presented in Sec. VII B allow the reconstruction of the DM-SFI operators $\hat{\mathbf{U}}^{\mathrm{R}}(I)$ in amplitude and phase from experimental transient-absorption spectra:

$$\left.\begin{matrix}\mathcal{S}_{\mathrm{exp}}(\omega,\tau)\\ \mathcal{S}_{\mathrm{fit}}(\omega,\tau,\mathbf{U}_{\mathrm{pu};ij,i'j'})\end{matrix}\right\}\xrightarrow[\text{fitting}]{}\text{Reconstructed operator }\hat{\mathbf{U}}^{\mathrm{R}}. \quad (41)$$

Here, in contrast to Sec. V, we solve the master equation (26) and calculate the time evolution of the density matrix $\hat{\rho}(t,\tau)$ when the system interacts with pump and probe pulses separated by a time delay τ. We assume decay rates $\gamma_{21}=\gamma_{31}=\gamma_{23}=1/(12\text{ ps})$ and $\gamma_{22}=\gamma_{33}=1/(720\text{ ps})$, in order to model experimental collision-induced and Doppler broadening [39]. We notice that all assumed decay rates, both for decoherence and population decay, are much larger than those for spontaneous decay in Rb, which is therefore neglected. At the same time, all decay times are much longer than the femtosecond duration of the pump and probe pulses employed. Details on the equations of motion used are provided in Appendix D. The solution of the equations of motion (27) is included into Eqs. (5) and (6), in order to numerically

simulate, with a full density-matrix formalism, experimental absorption spectra in the noncollinear geometry of Fig. 2(a) [21]. As already discussed in Sec. V, the spectra are calculated for pump-pulse intensities ranging from 0.1×10^{10} W/cm^2 to 5×10^{10} W/cm^2. The analytical model of Sec. VII B is then employed to fit the numerically simulated spectra and extract $\hat{\mathbf{U}}^{\mathrm{R}}(I)$. We stress that the fit parameters thereby extracted differ from those obtained in Sec. V, where spectra were used, which were calculated via a Schrödinger-like approach.

The reconstructed DM-SFI operators can then be employed to implement deterministic strong-field control based on Eq. (32). In analogy to Sec. V, we use a two-pulse scheme, and take advantage of the reconstructed DM-SFI operators $\hat{\mathbf{U}}^{\mathrm{R}}$ in order to control the populations $\rho_{2,ii}$, $i \in \{1, 2, 3\}$, of the final state $\hat{\rho}_2$, by optimizing the intensities I_m and the CEPs ϕ_m of the two control pulses, $m \in \{1, 2\}$, and the pulse separation $\bar{\tau}$. The reached final state thereby predicted $\hat{\rho}_{\mathrm{p}}$ has components given by

$$\rho_{\mathrm{p};ij} = \sum_{i'j'} \sum_{i''j''} \mathbf{U}^{\mathrm{R}}_{ij,i'j'}(I_2) \mathbf{\Phi}_{i'j',i'j'}(\bar{\phi}) \mathbf{W}_{i'j',i''j''}(\bar{\tau}) \mathbf{U}^{\mathrm{R}}_{i''j'',11}(I_1). \tag{42}$$

In Eq. (42), we have used the initial state $\hat{\rho}_0 = |1\rangle\langle 1|$, we have neglected phase operators not influencing the final populations, and defined the total phase $\bar{\phi} = \phi_2 - \phi_1 - \omega_{\mathrm{L}}\bar{\tau}$. Furthermore, we have introduced the slowly oscillating operator $\hat{\mathbf{W}}(\bar{\tau})$ such that $\mathbf{\Phi}_{ij,ij}(\bar{\phi}) \mathbf{W}_{ij,i'j'}(\bar{\tau}) = \mathbf{\Phi}_{ij,ij}(\phi_2) \mathbf{V}_{ij,i'j'}(\bar{\tau}) \mathbf{\Phi}^*_{i'j',i'j'}(\phi_1)$, with $\mathbf{\Phi}_{ij,ij}(\phi) = \Phi_{ii}(\phi)\Phi^*_{jj}(\phi)$.

To exemplify the effectiveness of our deterministic strong-field control method also when a density-matrix formalism is required, we focus on the same example discussed in Sec. V, and determine sequences of two strong pulses aiming at the desired final populations $(\rho_{\mathrm{d},11}, \rho_{\mathrm{d},22}, \rho_{\mathrm{d},33}) = (0, 2/3, 1/3)$. In this case, with a formalism directly based on density-matrix elements instead of quantum-state amplitudes, we do not need to introduce the free phase parameters δ and γ, as necessary in Sec. V. Also the free parameter A, associated with the total final population A^2 of the desired final state, does not have to be introduced here, since a density-matrix formalism ensures the conservation of the total population of the system $\rho_{11} + \rho_{22} + \rho_{33} = 1$. The pulse properties which optimally lead the system to the desired final state are determined by minimizing the cost function

$$g_\rho(I_1, I_2, \bar{\tau}, \bar{\phi}) = \sqrt{\sum_{i=1}^{3} |\rho_{\mathrm{d},ii} - \rho_{\mathrm{p},ii}|^2}, \tag{43}$$

which we calculate for a discrete set of parameters. Figure 5(a) shows the resulting dynamics of the system [Eq. (27)], when excited with the sequence of pulses determined via minimization of g_ρ, exhibiting very good agreement with the desired final state.

In order to compare these results, obtained with a density-matrix formalism, with those we previously discussed based on a Schrödinger-like approach, we display in Fig. 5(b) the dynamics of the system, solution of the equations of motion for the density matrix [Eq. (27)], when excited with the same sequence of pulses used in Fig. 3(c). That sequence of pulses was determined by minimizing the cost function g, based on a Schrödinger-like approach. Figure 5(b) displays very good agreement with the desired final state and with the results previously displayed in Fig. 3(c). This confirms the insensitivity of our operator-reconstruction and deterministic-control method to the details of dissipation, and justifies the Schrödinger-like approach developed and discussed in the previous sections for control time scales much shorter than the decay times of the system.

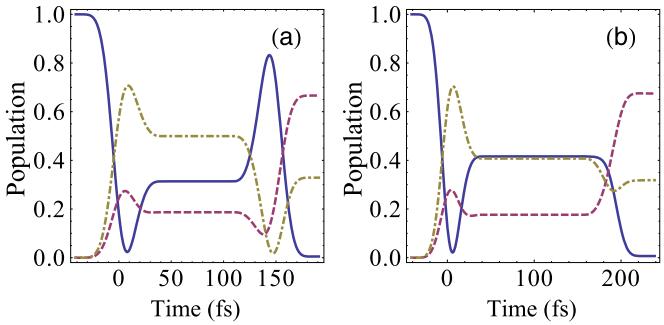

FIG. 5. Time evolution of the populations $\rho_{11}(t)$ (blue, continuous), $\rho_{22}(t)$ (purple, dashed), and $\rho_{33}(t)$ (yellow, dotdashed), of a three-level system modeling Rb atoms excited by a two-pulse control sequence, based on the reconstruction of density-matrix strong-field interaction operators. (a) Optimal pulse parameters are determined via minimization of Eq. (43), $I_1 = 2.9 \times 10^{10}$ W/cm^2, $I_2 = 3.2 \times 10^{10}$ W/cm^2, $\bar{\tau} = 150$ fs, and $\bar{\phi} = 1.13$ rad, with reached final populations $\rho_{\mathrm{r},11} = 0.00$, $\rho_{\mathrm{r},22} = 0.67$, and $\rho_{\mathrm{r},33} = 0.33$. (b) The same pulse parameters are used as in Fig. 3(c), $I_1 = 3.3 \times 10^{10}$ W/cm^2, $I_2 = 3.6 \times 10^{10}$ W/cm^2, $\bar{\tau} = 198$ fs, and $\bar{\phi} = 1.88$ rad, with reached final populations $\rho_{\mathrm{r},11} = 0.01$, $\rho_{\mathrm{r},22} = 0.67$, and $\rho_{\mathrm{r},33} = 0.32$.

VIII. CONCLUSION

In conclusion, we have designed an optimized sequence for quantum-state control based on intensity-dependent operators extractable from observable transient-absorption spectra. Schemes consisting of a higher number of pulses are possible to further enhance the control precision or to achieve additional control goals simultaneously. The method was mainly discussed for a three-level scheme modeling Rb atoms, but this could be generalized to higher numbers of states, potentially including the experimental characterization of the effect of chirp in terms of SFI operators, albeit with a scaling in complexity. By increasing the number of free control parameters, such as, e.g., chirp, additional experiments would have to be performed in order to characterize from TAS the dependence of the SFI operators on those supplemental variables. Furthermore, a higher number of excited states would imply several beating frequencies ω_{ij}, all contributing to the time-delay-dependent oscillations displayed by associated transient-absorption spectra. Hence, more complex analytical fitting models would have to be calculated, in order to distinguish contributions associated with different matrix elements of larger-dimensional SFI operators. Attention should also be paid in the presence of degenerate levels: however, in case these levels are characterized by different angular-momentum quantum numbers M, the polarization vector of the pulse could

be utilized as an additional degree of freedom for coherent control.

Our results are expected to trigger the development of related techniques for interaction-operator reconstruction of more complex systems such as molecules, for which strong-field absorption-line-shape control was recently demonstrated [34]. The advances in coherent x-ray sources open up interesting prospects especially for the application of our method at short wavelengths. Quantifying the effect of strong broadband pulses from experimentally accessible spectra would then enable quantum control based on designed sequences of the available, ultrashort x-ray pulses, with added benefits such as site specificity near core transitions.

ACKNOWLEDGMENTS

S.M.C. and Z.H. acknowledge helpful discussions with Jörg Evers and Christian Ott.

APPENDIX A: NUMERICAL SIMULATION OF THE QUANTUM DYNAMICS FOR A THREE- AND FIVE-LEVEL MODEL WITH A SCHRÖDINGER-LIKE APPROACH

We model Rb atoms as three- or five-level systems, as shown in Fig. 2(b), and solve the corresponding Schrödinger equation (2). For our calculations, pump and probe pulses are modeled via envelope functions of the form $f(t) = \cos^2(\pi t/T)\, R(t/T)$. Here, $R(x) = \theta(x+1/2) - \theta(x-1/2)$ is defined in terms of the Heaviside step function $\theta(x)$, such that $T = \pi T_{\mathrm{FWHM}}/[2\arccos(\sqrt[4]{1/2})]$, with T_{FWHM} being the full width at half maximum of $f^2(t)$. In this appendix, we employ a Schrödinger-equation-based formalism, with decay rates $\gamma_2 = \gamma_3 = 1/(1500\ \mathrm{fs})$ modeling experimental linewidths and included in the atomic-structure Hamiltonian $\hat{H}_0 = \sum_i (\omega_i - i\gamma_i/2)|i\rangle\langle i|$. In Sec. VII and Appendix D, we display how our results can be generalized to a more complex case requiring a density-matrix formulation.

To avoid repetitions, in the following we immediately refer to the more general case of a five-level scheme. The state of the system $|\psi^{(5)}(t,\tau)\rangle = \sum_{i=1}^{5} c_i^{(5)}(t,\tau)|i\rangle$ has a vector representation given by $\boldsymbol{c}^{(5)} = (c_1^{(5)}, c_2^{(5)}, c_3^{(5)}, c_4^{(5)}, c_5^{(5)})^{\mathrm{T}}$. The free-evolution operator is given by

$$\hat{V}^{(5)}(t) = \mathrm{diag}(1, e^{-[(\gamma_2/2)+i\omega_{21}]t}, e^{-[(\gamma_3/2)+i\omega_{31}]t}, e^{-[(\gamma_4/2)+i\omega_{41}]t}, e^{-[(\gamma_5/2)+i\omega_{51}]t}). \tag{A1}$$

Here, the two highest-lying excited states are almost degenerate, with transition energies $\omega_{41} = \omega_{51} = 3.19$ eV. For the $E1$-allowed transitions depicted in Fig. 2(b), we introduce the time-dependent Rabi frequencies $\Omega_{ij}(t) = D_{ij}\mathcal{E}_0 f(t)$, with dipole-moment matrix elements $\hat{\boldsymbol{D}}_{ij} = D_{ij}\hat{\boldsymbol{e}}_z$ aligned along the pulse polarization vector [41,42]. We calculate the time evolution of the atomic system interacting with a pump pulse centered on $t_{\mathrm{c,pu}} = 0$ and a probe pulse centered on $t_{\mathrm{c,pr}} = \tau$. Both pulses are transform limited, and no chirp is included. We assume a weak probe pulse, with duration $T_{\mathrm{FWHM,pr}} = 15$ fs and intensity $I_{\mathrm{pr}} = 1\times10^8\ \mathrm{W/cm^2}$, and pump pulses of duration $T_{\mathrm{FWHM,pu}} = 30$ fs and intensities I_{pu} varying between $0.1\times10^{10}\ \mathrm{W/cm^2}$ and $5\times10^{10}\ \mathrm{W/cm^2}$. For $(t-t_{\mathrm{c}}) \in [-T/2, T/2]$, the time evolution of $\boldsymbol{c}^{(5)}$ in the rotating-wave approximation is given by

$$\frac{d\boldsymbol{c}^{(5)}}{dt} = [\hat{\Phi}^{(5)}(\phi)]^{\dagger}[\hat{\Lambda}^{(5)}(t-t_{\mathrm{c}})]^{\dagger}\hat{M}^{(5)}(t-t_{\mathrm{c}})\hat{\Lambda}^{(5)}(t-t_{\mathrm{c}}) \times \hat{\Phi}^{(5)}(\phi)\boldsymbol{c}^{(5)}(t), \tag{A2}$$

with the phase of the pulse accounted for by $\hat{\Phi}^{(5)}(\phi) = \mathrm{diag}(1, e^{i\phi}, e^{i\phi}, e^{2i\phi}, e^{2i\phi})$ and $\hat{\Lambda}^{(5)}(t) = \mathrm{diag}(1, e^{i\omega_{\mathrm{L}}t}, e^{i\omega_{\mathrm{L}}t}, e^{2i\omega_{\mathrm{L}}t}, e^{2i\omega_{\mathrm{L}}t})$, while

$$\hat{M}^{(5)}(t) = \begin{pmatrix} 0 & i\frac{\Omega_{12}(t)}{2} & i\frac{\Omega_{13}(t)}{2} & 0 & 0 \\ i\frac{\Omega_{12}^*(t)}{2} & -\frac{\gamma_2}{2} - i\omega_{21} & 0 & i\frac{\Omega_{24}(t)}{2} & 0 \\ i\frac{\Omega_{13}^*(t)}{2} & 0 & -\frac{\gamma_3}{2} - i\omega_{31} & i\frac{\Omega_{34}(t)}{2} & i\frac{\Omega_{35}(t)}{2} \\ 0 & i\frac{\Omega_{24}^*(t)}{2} & i\frac{\Omega_{34}^*(t)}{2} & -\frac{\gamma_4+\gamma_{\mathrm{P},4}(t)}{2} - i\omega_{41} & 0 \\ 0 & 0 & i\frac{\Omega_{35}^*(t)}{2} & 0 & -\frac{\gamma_5+\gamma_{\mathrm{P},5}(t)}{2} - i\omega_{51} \end{pmatrix}. \tag{A3}$$

Photoionization of states $|4\rangle$ and $|5\rangle$ in the presence of an optical pulse has also been included as an effective loss of amplitude at the rate $\gamma_{\mathrm{P},l}(t) = \sigma_l(\omega_{\mathrm{L}})\mathcal{I}_{\mathrm{L}}(t)$, with photoionization cross sections $\sigma_l(\omega_{\mathrm{L}})$ calculated with [44], and optical flux $\mathcal{I}_{\mathrm{L}}(t) = I_{\mathrm{L}}(t)/\omega_{\mathrm{L}}$ defined in terms of the time-dependent pulse intensity $I_{\mathrm{L}}(t) = [\mathcal{E}_0 f(t)]^2/(8\pi\alpha)$.

The dynamics of the five-level system are associated with the 5×5 evolution operator $\hat{\mathcal{U}}^{(5)}(t,t_0)$ and the related interaction operator

$$\hat{U}^{(5)} = \hat{V}^{(5)}(-T/2)\hat{\mathcal{U}}_0^{(5)}(T/2,-T/2)[\hat{V}^{(5)}(T/2)]^{-1} = \begin{pmatrix} \hat{U}_{3\times3}^{(5)} & \hat{U}_{3\times2}^{(5)} \\ \hat{U}_{2\times3}^{(5)} & \hat{U}_{2\times2}^{(5)} \end{pmatrix}. \tag{A4}$$

The time evolution of the five-level system, calculated from Eq. (A2), is used to numerically simulate transient-absorption spectra $\mathcal{S}^{(5)}(\omega,\tau)$ via Eqs. (4) and (6).

For a three-level model associated with the state $|\psi^{(3)}(t,\tau)\rangle = \sum_{i=1}^{3} c_i^{(3)}(t,\tau)|i\rangle$, the dynamics of the system are described in terms of the operators $\hat{V}^{(3)}(t) = \mathrm{diag}(1, e^{-[(\gamma_2/2)+i\omega_{21}]t}, e^{-[(\gamma_3/2)+i\omega_{31}]t})$, $\hat{\Phi}^{(3)}(\phi) = \mathrm{diag}(1, e^{i\phi}, e^{i\phi})$, $\hat{\Lambda}^{(3)}(t) = \mathrm{diag}(1, e^{i\omega_{\mathrm{L}}t}, e^{i\omega_{\mathrm{L}}t})$, while

$$\hat{M}^{(3)}(t) = \begin{pmatrix} 0 & i\frac{\Omega_{12}(t)}{2} & i\frac{\Omega_{13}(t)}{2} \\ i\frac{\Omega_{12}^*(t)}{2} & -\frac{\gamma_2}{2} - i\omega_{21} & 0 \\ i\frac{\Omega_{13}^*(t)}{2} & 0 & -\frac{\gamma_3}{2} - i\omega_{31} \end{pmatrix}, \tag{A5}$$

resulting in a 3×3 evolution operator $\hat{\mathcal{U}}^{(3)}(t,t_0)$ and a related interaction operator $\hat{U}^{(3)} = \hat{V}^{(3)}(-T/2)\hat{\mathcal{U}}_0^{(3)}(T/2,-T/2)[\hat{V}^{(3)}(T/2)]^{-1}$. It is important to stress that the 3×3 matrix $\hat{U}^{(5)}_{3\times3}$ is different from $\hat{U}^{(3)}$, since $\hat{U}^{(5)}_{3\times3}$ is influenced by the presence of states $|4\rangle$ and $|5\rangle$, which could not be taken into account if one solved the Schrödinger equation for a three-level system exclusively. By using TAS to extract SFI operators by means of the analytical fitting model presented in Sec. IV, one has thus access to $\hat{U}^{(5)}_{3\times3}$, in contrast to methods based exclusively on a theory which could only provide $\hat{U}^{(3)}$.

APPENDIX B: INTERACTION OPERATOR FOR WEAK, SHORT PROBE PULSES

In order to interpret results from TAS, the interaction operator $\hat{U}_{\rm pr}$ was introduced in Eq. (7), modeling the action of a weak probe pulse, with FWHM of 15 fs and intensity of 1×10^8 W/cm^2. In order to derive Eq. (7), we consider a Dirac-δ-like peak

$$\tilde{f}_{\rm pr}(t) = \delta(t) \int_{-T_{\rm pr}/2}^{T_{\rm pr}/2} f_{\rm pr}(t')dt', \tag{B1}$$

where $f_{\rm pr}(t)$ is the actual envelope of the short (broadband), weak probe pulse used in our numerical simulations, and $T_{\rm pr}$ is the associated pulse duration.

An explicit solution of Eq. (2) for the pulse envelope in Eq. (B1) provides

$$\hat{\mathcal{U}}_{\rm pr}(t,t_0) = \hat{V}(t)e^{\hat{B}[\theta(t)-\theta(t_0)]}\hat{V}(-t_0), \tag{B2}$$

where $\theta(x)$ is the Heaviside step function, $\hat{V}(t)$ is the free-evolution operator, and

$$\hat{B} = \begin{pmatrix} 0 & i\frac{\vartheta_2}{2} & i\frac{\vartheta_3}{2} \\ i\frac{\vartheta_2^*}{2} & 0 & 0 \\ i\frac{\vartheta_3^*}{2} & 0 & 0 \end{pmatrix} \tag{B3}$$

is defined in terms of the pulse areas $\vartheta_k = \int_{-T_{\rm pr}/2}^{T_{\rm pr}/2} \Omega_{{\rm pr},1k}(t)dt$ of the probe-pulse Rabi frequencies $\Omega_{{\rm pr},1k}(t)$, for $k \in \{2, 3\}$. Taking advantage of the weak probe-pulse intensity, the probe operator $\hat{U}_{\rm pr} = \hat{V}(-T_{\rm pr}/2)\hat{\mathcal{U}}_{\rm pr}(T_{\rm pr}/2, -T_{\rm pr}/2)\hat{V}^{-1}(T_{\rm pr}/2)$ reads

$$\hat{U}_{\rm pr} = e^{\hat{B}} \approx \hat{I}_3 + \hat{B} = \begin{pmatrix} 1 & i\frac{\vartheta_2}{2} & i\frac{\vartheta_3}{2} \\ i\frac{\vartheta_2^*}{2} & 1 & 0 \\ i\frac{\vartheta_3^*}{2} & 0 & 1 \end{pmatrix}. \tag{B4}$$

APPENDIX C: SYMMETRIC STRONG-FIELD INTERACTION OPERATORS

In order to independently extract $U_{{\rm pu},12}$ and $U_{{\rm pu},13}$ in a noncollinear geometry, we here show that, when the envelope function $f(t) = f(-t)$ is a symmetric function of time, then the associated interaction operator $\hat{U} = \hat{V}(-T/2)\hat{\mathcal{U}}_0(T/2, -T/2)\hat{V}^{-1}(T/2)$ is a symmetric matrix. By using Eq. (A2) for a three-level system and by recalling that the time evolution of $\hat{\mathcal{U}}_0(t,t_0)$ is calculated for a pulse with $\phi = 0$ and $t_c = 0$, we obtain that

$$\frac{d\hat{\mathcal{U}}_0(t,t_0)}{dt} = [\hat{\Lambda}^{(3)}(t)]^\dagger \hat{M}^{(3)}(t)\hat{\Lambda}^{(3)}(t)\hat{\mathcal{U}}(t,t_0),$$
$$\hat{\mathcal{U}}(t_0,t_0) = \hat{I}. \tag{C1}$$

The assumption of a symmetric envelope, $f(t) = f(-t)$, implies that also $\hat{M}^{(3)}(t)$ is symmetric in time.

We thus introduce the operator $\hat{\mathcal{Z}}(t,t_0) = \hat{\mathcal{U}}_0(-t,-t_0)$, which is solution of the differential equation

$$\frac{d\hat{\mathcal{Z}}(t,t_0)}{dt} = -\hat{\Lambda}^{(3)}(t)\hat{M}^{(3)}(t)[\hat{\Lambda}^{(3)}(t)]^{-1}\hat{\mathcal{Z}}(t,t_0),$$
$$\hat{\mathcal{Z}}(t_0,t_0) = \hat{I}, \tag{C2}$$

where $\hat{\Lambda}^{(3)}(-t) = [\hat{\Lambda}^{(3)}(t)]^{-1}$ and $\hat{M}^{(3)}(-t) = \hat{M}^{(3)}(t)$. Both $\hat{\Lambda}^{(3)}(t) = [\hat{\Lambda}^{(3)}(t)]^{\rm T}$ and $\hat{M}^{(3)}(t) = [\hat{M}^{(3)}(t)]^{\rm T}$ are symmetric matrices. As a result,

$$\frac{d\hat{\mathcal{Z}}^{-1}(t,t_0)}{dt} = \hat{\mathcal{Z}}^{-1}(t,t_0)\hat{\Lambda}^{(3)}(t)\hat{M}^{(3)}(t)[\hat{\Lambda}^{(3)}(t)]^{-1},$$
$$\hat{\mathcal{Z}}^{-1}(t_0,t_0) = \hat{I} \tag{C3}$$

and

$$\frac{d(\hat{\mathcal{Z}}^{-1})^{\rm T}(t,t_0)}{dt} = [\hat{\Lambda}^{(3)}(t)]^{-1}\hat{M}^{(3)}(t)\hat{\Lambda}^{(3)}(t)[(\hat{\mathcal{Z}}^{-1})^{\rm T}(t,t_0)],$$
$$(\hat{\mathcal{Z}}^{-1})^{\rm T}(t_0,t_0) = \hat{I}. \tag{C4}$$

Since this equation corresponds to Eq. (C1), the evolution operators $(\hat{\mathcal{Z}}^{-1})^{\rm T}(t,t_0)$ and $\hat{\mathcal{U}}_0(t,t_0)$ are solutions of the same differential equations and are therefore identical, and hence $\hat{\mathcal{U}}_0(T/2,0) = \hat{\mathcal{U}}_0^{-1}(0,T/2) = \hat{\mathcal{Z}}^{-1}(0,-T/2) = \hat{\mathcal{U}}_0^{\rm T}(0,-T/2)$. As a result,

$$\hat{\mathcal{U}}_0(T/2,-T/2) = \hat{\mathcal{U}}_0(T/2,0)\hat{\mathcal{U}}_0(0,-T/2)$$
$$= \hat{\mathcal{U}}_0^{\rm T}(0,-T/2)\hat{\mathcal{U}}_0(0,-T/2) \tag{C5}$$

and

$$\hat{\mathcal{U}}_0^{\rm T}(T/2,-T/2) = \hat{\mathcal{U}}_0^{\rm T}(0,-T/2)\hat{\mathcal{U}}_0(0,-T/2)$$
$$= \hat{\mathcal{U}}_0(T/2,-T/2), \tag{C6}$$

i.e., $\hat{\mathcal{U}}_0(T/2,-T/2)$ is a symmetric matrix. Since $\hat{V}(t)$ is a diagonal (and therefore symmetric) matrix, it follows that $\hat{U} = \hat{V}(-T/2)\hat{\mathcal{U}}_0(T/2,-T/2)\hat{V}^{-1}(T/2)$ is symmetric.

We hence use the above result for the operator $\hat{U}_{\rm pu}$ reconstructed from strong-field TAS, and fix $U_{{\rm pu},1k} = U_{{\rm pu},k1}$.

APPENDIX D: EQUATIONS OF MOTION WITH A DENSITY-MATRIX FORMALISM

In this appendix, we provide the explicit form of the set of differential equations (27) satisfied by the 3×3 density matrix $\hat{\rho}(t)$, modeling the evolution of the three-level system in the blue box in Fig. 2(b) interacting with pump and probe pulses. Here, the pulses are modeled via envelope functions of the form $f(t) = \cos^2(\pi t/T)\, R(t/T)$, where $R(x) = \theta(x + 1/2) - \theta(x - 1/2)$ is defined in terms of the Heaviside step function $\theta(x)$, such that $T = \pi T_{\rm FWHM}/[2\arccos(\sqrt[4]{1/2})]$, with $T_{\rm FWHM}$ being the full width at half maximum of $f^2(t)$.

We write the equations of motion explicitly in matrix form. For this purpose, we first introduce the vectors

$\vec{\rho}_i = (\rho_{i1}, \rho_{i2}, \rho_{i3})^{\mathrm{T}}$, $i \in \{1, 2, 3\}$, whose components are the elements of the ith row of the density matrix $\hat{\rho}$. This allows us to introduce the nine-dimensional vector

$$\vec{\vec{\rho}} = \begin{pmatrix} \vec{\rho}_1 \\ \vec{\rho}_2 \\ \vec{\rho}_3 \end{pmatrix}. \tag{D1}$$

For any operator $\hat{\mathbf{A}}$ acting on the elements of the density matrix as, e.g., $\sum_{i'j'} \mathbf{A}_{ij,i'j'} \rho_{i'j'}$, we analogously define the 3×3 matrices

$$\bar{\mathbf{A}}_{ii'} = \begin{pmatrix} \mathbf{A}_{i1,i'1} & \mathbf{A}_{i1,i'2} & \mathbf{A}_{i1,i'3} \\ \mathbf{A}_{i2,i'1} & \mathbf{A}_{i2,i'2} & \mathbf{A}_{i2,i'3} \\ \mathbf{A}_{i3,i'1} & \mathbf{A}_{i3,i'2} & \mathbf{A}_{i3,i'3} \end{pmatrix}, \tag{D2}$$

$i,i' \in \{1,2,3\}$, which we use to introduce the 9×9 matrix

$$\bar{\bar{\mathbf{A}}} = \begin{pmatrix} \bar{\mathbf{A}}_{11} & \bar{\mathbf{A}}_{12} & \bar{\mathbf{A}}_{13} \\ \bar{\mathbf{A}}_{21} & \bar{\mathbf{A}}_{22} & \bar{\mathbf{A}}_{23} \\ \bar{\mathbf{A}}_{31} & \bar{\mathbf{A}}_{32} & \bar{\mathbf{A}}_{33} \end{pmatrix}. \tag{D3}$$

In the presence of a pulse centered on t_c and with duration T, i.e., for $(t - t_c) \in [-T/2, T/2]$, the equations of motion (27) can be written in matrix form as

$$\frac{d\vec{\vec{\rho}}(t)}{dt} = \bar{\bar{\mathfrak{M}}}(t)\vec{\vec{\rho}}(t), \tag{D4}$$

$$\bar{\bar{\mathfrak{M}}}(t) = [\bar{\bar{\mathbf{\Phi}}}(\phi)]^{\dagger}[\bar{\bar{\mathbf{\Lambda}}}(t - t_c)]^{\dagger}\bar{\bar{\mathbf{M}}}(t - t_c)\bar{\bar{\mathbf{\Lambda}}}(t - t_c)\bar{\bar{\mathbf{\Phi}}}(\phi), \tag{D5}$$

generalizing Eq. (A2) to a density-matrix formalism. Specifically,

$$\bar{\bar{\mathbf{\Phi}}}(\phi) = \mathrm{diag}(1, e^{-i\phi}, e^{-i\phi}, e^{i\phi}, 1, 1, e^{i\phi}, 1, 1) \tag{D6}$$

and

$$\bar{\bar{\mathbf{\Lambda}}}(t) = \mathrm{diag}(1, e^{-i\omega_L t}, e^{-i\omega_L t}, e^{i\omega_L t}, 1, 1, e^{i\omega_L t}, 1, 1), \tag{D7}$$

whereas

$$\bar{\bar{\mathbf{M}}}(t) = \begin{pmatrix} 0 & -i\frac{\Omega_{12}^*(t)}{2} & -i\frac{\Omega_{13}^*(t)}{2} & i\frac{\Omega_{12}(t)}{2} & \gamma_{22} & 0 & i\frac{\Omega_{13}(t)}{2} & 0 & \gamma_{33} \\ -i\frac{\Omega_{12}(t)}{2} & -\gamma_{21} + i\omega_{21} & 0 & 0 & i\frac{\Omega_{12}(t)}{2} & 0 & 0 & i\frac{\Omega_{13}(t)}{2} & 0 \\ -i\frac{\Omega_{13}(t)}{2} & 0 & -\gamma_{31} + i\omega_{31} & 0 & 0 & i\frac{\Omega_{12}(t)}{2} & 0 & 0 & i\frac{\Omega_{13}(t)}{2} \\ i\frac{\Omega_{12}^*(t)}{2} & 0 & 0 & -\gamma_{21} - i\omega_{21} & -i\frac{\Omega_{12}^*(t)}{2} & -i\frac{\Omega_{13}^*(t)}{2} & 0 & 0 & 0 \\ 0 & i\frac{\Omega_{12}^*(t)}{2} & 0 & -i\frac{\Omega_{12}(t)}{2} & -\gamma_{22} & 0 & 0 & 0 & 0 \\ 0 & 0 & i\frac{\Omega_{12}^*(t)}{2} & -i\frac{\Omega_{13}(t)}{2} & 0 & -\gamma_{23} + i\omega_{32} & 0 & 0 & 0 \\ i\frac{\Omega_{13}^*(t)}{2} & 0 & 0 & 0 & 0 & 0 & -\gamma_{31} - i\omega_{31} & -i\frac{\Omega_{12}^*(t)}{2} & -i\frac{\Omega_{13}^*(t)}{2} \\ 0 & i\frac{\Omega_{13}^*(t)}{2} & 0 & 0 & 0 & 0 & -i\frac{\Omega_{12}(t)}{2} & -\gamma_{23} - i\omega_{32} & 0 \\ 0 & 0 & i\frac{\Omega_{13}^*(t)}{2} & 0 & 0 & 0 & -i\frac{\Omega_{13}(t)}{2} & 0 & -\gamma_{33} \end{pmatrix}. \tag{D8}$$

The free-evolution operator $\hat{\mathbf{V}}(t)$ is associated with the matrix

$$\bar{\bar{\mathbf{V}}}(t) = \begin{pmatrix} 1 & 0 & 0 & 0 & 1 - e^{-\gamma_{22}t} & 0 & 0 & 0 & 1 - e^{-\gamma_{33}t} \\ 0 & e^{-\gamma_{21}t}e^{i\omega_{21}t} & 0 & 0 & 0 & 0 & 0 & 0 & 0 \\ 0 & 0 & e^{-\gamma_{31}t}e^{i\omega_{31}t} & 0 & 0 & 0 & 0 & 0 & 0 \\ 0 & 0 & 0 & e^{-\gamma_{21}t}e^{-i\omega_{21}t} & 0 & 0 & 0 & 0 & 0 \\ 0 & 0 & 0 & 0 & e^{-\gamma_{22}t} & 0 & 0 & 0 & 0 \\ 0 & 0 & 0 & 0 & 0 & e^{-\gamma_{23}t}e^{i\omega_{32}t} & 0 & 0 & 0 \\ 0 & 0 & 0 & 0 & 0 & 0 & e^{-\gamma_{31}t}e^{-i\omega_{31}t} & 0 & 0 \\ 0 & 0 & 0 & 0 & 0 & 0 & 0 & e^{-\gamma_{23}t}e^{-i\omega_{32}t} & 0 \\ 0 & 0 & 0 & 0 & 0 & 0 & 0 & 0 & e^{-\gamma_{33}t} \end{pmatrix}. \tag{D9}$$

Assuming that the density-matrix probe-pulse operator $\hat{\mathbf{U}}_{\rm pr} = \hat{U}_{\rm pr} \otimes \hat{U}^*_{\rm pr}$ can be factorized in terms of the operator (7) calculated in first-order perturbation theory in Appendix B, $\hat{\mathbf{U}}_{\rm pr}$ is associated with the matrix

$$\bar{\bar{\mathbf{U}}}_{\rm pr} = \begin{pmatrix} 1 & -i\frac{\vartheta_2^*}{2} & -i\frac{\vartheta_3^*}{2} & i\frac{\vartheta_2}{2} & 0 & 0 & i\frac{\vartheta_3}{2} & 0 & 0 \\ -i\frac{\vartheta_2}{2} & 1 & 0 & 0 & i\frac{\vartheta_2}{2} & 0 & 0 & i\frac{\vartheta_3}{2} & 0 \\ -i\frac{\vartheta_3}{2} & 0 & 1 & 0 & 0 & i\frac{\vartheta_2}{2} & 0 & 0 & i\frac{\vartheta_3}{2} \\ i\frac{\vartheta_2^*}{2} & 0 & 0 & 1 & -i\frac{\vartheta_2^*}{2} & -i\frac{\vartheta_3^*}{2} & 0 & 0 & 0 \\ 0 & i\frac{\vartheta_2^*}{2} & 0 & -i\frac{\vartheta_2}{2} & 1 & 0 & 0 & 0 & 0 \\ 0 & 0 & i\frac{\vartheta_2^*}{2} & -i\frac{\vartheta_3}{2} & 0 & 1 & 0 & 0 & 0 \\ i\frac{\vartheta_3^*}{2} & 0 & 0 & 0 & 0 & 0 & 1 & -i\frac{\vartheta_2^*}{2} & -i\frac{\vartheta_3^*}{2} \\ 0 & i\frac{\vartheta_3^*}{2} & 0 & 0 & 0 & 0 & -i\frac{\vartheta_2}{2} & 1 & 0 \\ 0 & 0 & i\frac{\vartheta_3^*}{2} & 0 & 0 & 0 & -i\frac{\vartheta_3}{2} & 0 & 1 \end{pmatrix}. \tag{D10}$$

[1] C. Brif, R. Chakrabarti, and H. Rabitz, Control of quantum phenomena: Past, present and future, New J. Phys. **12**, 075008 (2010).

[2] D. J. Tannor, *Introduction to Quantum Mechanics: A Time-Dependent Perspective* (University Science Books, Sausalito, CA, 2007).

[3] A. P. Peirce, M. A. Dahleh, and H. Rabitz, Optimal control of quantum-mechanical systems: Existence, numerical approximation, and applications, Phys. Rev. A **37**, 4950 (1988).

[4] P. Brumer and M. Shapiro, Laser control of molecular processes, Annu. Rev. Phys. Chem. **43**, 257 (1992).

[5] R. S. Judson and H. Rabitz, Teaching Lasers to Control Molecules, Phys. Rev. Lett. **68**, 1500 (1992).

[6] D. Meshulach and Y. Silberberg, Coherent quantum control of two-photon transitions by a femtosecond laser pulse, Nature (London) **396**, 239 (1998).

[7] T. C. Weinacht, J. Ahn, and P. H. Bucksbaum, Controlling the shape of a quantum wavefunction, Nature (London) **397**, 233 (1999).

[8] T. Brixner, N. H. Damrauer, P. Niklaus, and G. Gerber, Photoselective adaptive femtosecond quantum control in the liquid phase, Nature (London) **414**, 57 (2001).

[9] C. Daniel, J. Full, L. González, C. Lupulescu, J. Manz, A. Merli, Š. Vajda, and L. Wöste, Deciphering the reaction dynamics underlying optimal control laser fields, Science **299**, 536 (2003).

[10] R. Rey-de-Castro, Z. Leghtas, and H. Rabitz, Manipulating Quantum Pathways on the Fly, Phys. Rev. Lett. **110**, 223601 (2013).

[11] N. Dudovich, T. Polack, A. Pe'er, and Y. Silberberg, Simple Route to Strong-Field Coherent Control, Phys. Rev. Lett. **94**, 083002 (2005).

[12] S. D. Clow, C. Trallero-Herrero, T. Bergeman, and T. Weinacht, Strong Field Multiphoton Inversion of a Three-Level System Using Shaped Ultrafast Laser Pulses, Phys. Rev. Lett. **100**, 233603 (2008).

[13] T. Bayer, M. Wollenhaupt, C. Sarpe-Tudoran, and T. Baumert, Robust Photon Locking, Phys. Rev. Lett. **102**, 023004 (2009).

[14] B. D. Bruner, H. Suchowski, N. V. Vitanov, and Y. Silberberg, Strong-field spatiotemporal ultrafast coherent control in three-level atoms, Phys. Rev. A **81**, 063410 (2010).

[15] C. Pellegrini, A. Marinelli, and S. Reiche, The physics of x-ray free-electron lasers, Rev. Mod. Phys. **88**, 015006 (2016).

[16] J. Amann, W. Berg, V. Blank, F.-J. Decker, Y. Ding, P. Emma, Y. Feng, J. Frisch, D. Fritz, J. Hastings *et al.*, Demonstration of self-seeding in a hard-x-ray free-electron laser, Nat. Photon. **6**, 693 (2012).

[17] E. Allaria, R. Appio, L. Badano, W. A. Barletta, S. Bassanese, S. G. Biedron, A. Borga, E. Busetto, D. Castronovo, P. Cinquegrana *et al.*, Highly coherent and stable pulses from the FERMI seeded free-electron laser in the extreme ultraviolet, Nat. Photon. **6**, 699 (2012).

[18] B. W. Adams, C. Buth, S. M. Cavaletto, J. Evers, Z. Harman, C. H. Keitel, A. Pálffy, A. Picón, R. Röhlsberger, Y. Rostovtsev, and K. Tamasaku, X-ray quantum optics, J. Mod. Opt. **60**, 2 (2013).

[19] D. Gauthier, P. R. Ribič, G. De Ninno, E. Allaria, P. Cinquegrana, M. B. Danailov, A. Demidovich, E. Ferrari, L. Giannessi, B. Mahieu, and G. Penco, Spectrotemporal Shaping of Seeded Free-Electron Laser Pulses, Phys. Rev. Lett. **115**, 114801 (2015).

[20] K. C. Prince, E. Allaria, C. Callegari, R. Cucini, G. De Ninno, S. Di Mitri, B. Diviacco, E. Ferrari, P. Finetti, D. Gauthier *et al.*, Coherent control with a short-wavelength free-electron laser, Nat. Photon. **10**, 176 (2016).

[21] Z. Liu, S. M. Cavaletto, C. Ott, K. Meyer, Y. Mi, Z. Harman, C. H. Keitel, and T. Pfeifer, Phase Reconstruction of Strong-Field Excited Systems by Transient-Absorption Spectroscopy, Phys. Rev. Lett. **115**, 033003 (2015).

[22] R. Santra, V. S. Yakovlev, T. Pfeifer, and Z.-H. Loh, Theory of attosecond transient absorption spectroscopy of strong-field-generated ions, Phys. Rev. A **83**, 033405 (2011).

[23] A. Blättermann, C. Ott, A. Kaldun, T. Ding, and T. Pfeifer, Two-dimensional spectral interpretation of time-dependent absorption near laser-coupled resonances, J. Phys. B **47**, 124008 (2014).

[24] M. O. Scully and M. S. Zubairy, *Quantum Optics* (Cambridge University Press, Cambridge, 1997).

[25] J. C. Diels and W. Rudolph, *Ultrashort Laser Pulse Phenomena: Fundamentals, Techniques, And Applications on a Femtosecond Time Scale* (Academic, Burlington, MA, 2006).

[26] R. A. Mathies, C. H. Brito Cruz, W. T. Pollard, and C. V. Shank, Direct observation of the femtosecond excited-state cis-trans isomerization in bacteriorhodopsin, Science **240**, 777 (1988).

[27] W. T. Pollard and R. A. Mathies, Analysis of femtosecond dynamic absorption spectra of nonstationary states, Annu. Rev. Phys. Chem. **43**, 497 (1992).

[28] Z.-H. Loh, M. Khalil, R. E. Correa, R. Santra, C. Buth, and S. R. Leone, Quantum State-Resolved Probing of Strong-Field-Ionized Xenon Atoms Using Femtosecond High-Order Harmonic Transient Absorption Spectroscopy, Phys. Rev. Lett. **98**, 143601 (2007).

[29] H. Wang, M. Chini, S. Chen, C.-H. Zhang, F. He, Y. Cheng, Y. Wu, U. Thumm, and Z. Chang, Attosecond Time-Resolved Autoionization of Argon, Phys. Rev. Lett. **105**, 143002 (2010).

[30] E. Goulielmakis, Z.-H. Loh, A. Wirth, R. Santra, N. Rohringer, V. S. Yakovlev, S. Zherebtsov, T. Pfeifer, A. M. Azzeer, M. F. Kling, S. R. Leone, and F. Krausz, Real-time observation of valence electron motion, Nature (London) **466**, 739 (2010).

[31] M. Holler, F. Schapper, L. Gallmann, and U. Keller, Attosecond Electron Wave-Packet Interference Observed by Transient Absorption, Phys. Rev. Lett. **106**, 123601 (2011).

[32] C. Ott, A. Kaldun, P. Raith, K. Meyer, M. Laux, J. Evers, C. H. Keitel, C. H. Greene, and T. Pfeifer, Lorentz meets Fano in spectral line shapes: A universal phase and its laser control, Science **340**, 716 (2013).

[33] M. Wu, S. Chen, S. Camp, K. J. Schafer, and M. B. Gaarde, Theory of strong-field attosecond transient absorption, J. Phys. B **49**, 062003 (2016).

[34] K. Meyer, Z. Liu, N. Müller, J.-M. Mewes, A. Dreuw, T. Buckup, M. Motzkus, and T. Pfeifer, Signatures and control of strong-field dynamics in a complex system, Proc. Natl. Acad. Sci. USA **112**, 15613 (2015).

[35] U. Fano and J. W. Cooper, Spectral distribution of atomic oscillator strengths, Rev. Mod. Phys. **40**, 441 (1968).

[36] S. Chen, M. J. Bell, A. R. Beck, H. Mashiko, M. Wu, A. N. Pfeiffer, M. B. Gaarde, D. M. Neumark, S. R. Leone, and K. J. Schafer, Light-induced states in attosecond transient absorption spectra of laser-dressed helium, Phys. Rev. A **86**, 063408 (2012).

[37] A. R. Beck, B. Bernhardt, E. R. Warrick, M. Wu, S. Chen, M. B. Gaarde, K. J. Schafer, D. M. Neumark, and S. R. Leone, Attosecond transient absorption probing of electronic superpositions of bound states in neon: Detection of quantum beats, New J. Phys. **16**, 113016 (2014).

[38] A. Kaldun, C. Ott, A. Blättermann, M. Laux, K. Meyer, T. Ding, A. Fischer, and T. Pfeifer, Extracting Phase and Amplitude Modifications of Laser-Coupled Fano Resonances, Phys. Rev. Lett. **112**, 103001 (2014).

[39] R. Netz, T. Feurer, G. Roberts, and R. Sauerbrey, Coherent population dynamics of a three-level atom in spacetime, Phys. Rev. A **65**, 043406 (2002).

[40] C. E. Theodosiou, Lifetimes of alkali-metal–atom Rydberg states, Phys. Rev. A **30**, 2881 (1984).

[41] S. B. Bayram, M. Havey, M. Rosu, A. Sieradzan, A. Derevianko, and W. R. Johnson, $5p^2P_j \rightarrow 5d^2D_{3/2}$ transition matrix elements in atomic ^{87}Rb, Phys. Rev. A **61**, 050502 (2000).

[42] M. S. Safronova, C. J. Williams, and C. W. Clark, Relativistic many-body calculations of electric-dipole matrix elements, lifetimes, and polarizabilities in rubidium, Phys. Rev. A **69**, 022509 (2004).

[43] For instance, since the ionization potential of states $|4\rangle$ and $|5\rangle$ is 0.98 eV, a laser tuned to (or slightly above) this energy would decrease population and coherence of these two excited states, without effectively affecting the remaining transitions at energies larger than 1.56 eV.

[44] Los Alamos National Laboratory Atomic Physics Codes, http://aphysics2.lanl.gov/tempweb.

[45] N. Dudovich, B. Dayan, S. M. Gallagher Faeder, and Y. Silberberg, Transform-Limited Pulses Are Not Optimal for Resonant Multiphoton Transitions, Phys. Rev. Lett. **86**, 47 (2001).